Modeling the electronic properties of π-conjugated self-assembled monolayers

By *Georg Heimel*,Ferdinand Rissner*, and *Egbert Zojer**

[*] Dr. G. Heimel
Institut für Physik
Humboldt-Universität zu Berlin
Newtonstrasse 15, 12389 Berlin (Germany)
E-mail: georg.heimel@physik.hu-berlin.de

[*] Prof. E. Zojer, F. Rissner
Institute of Solid State Physics
Graz University of Technology
Petersgasse 16, 8010 Graz (Austria)
E-mail: egbert.zojer@tugraz.at

Keywords: Electronic Structure, Self Assembly, Monolayers, Organic Electronics, Structure-Property Relationships

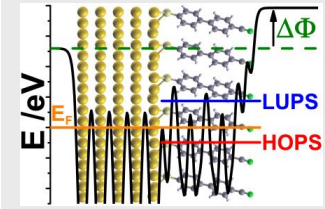

The modification of electrode surfaces by depositing self-assembled monolayers (SAMs) provides the possibility for controlled adjustment of various key parameters in organic and molecular electronic devices. Most important among them are the work-function of the electrode and the relative alignment of its Fermi level with the conducting states in the SAM itself and with those in a subsequently deposited organic semiconductor. For the efficient application of such interface modifications it is crucial to reach a proper understanding of the relation between the chemical structure of a molecule, its molecular electronic characteristics, and the properties a SAM formed by such molecules. Over the past years, quantum-mechanical calculations have proven to be a valuable tool for reaching a fundamental understanding of the relevant structure-property relations. Here, we provide a review over the field and report on recent progress in the modeling of the interfacial electronic properties of π-conjugated SAMs. In addition to the insight that can be gained from simple electrostatic considerations, we focus on the quantum-mechanical description of the roles played by substituents, molecular backbones, chemical anchoring groups, and the packing density of molecules on the surface. Furthermore, we explicitly address the energy-level alignment at the interface between a prototypical organic semiconductor and a SAM-covered metal electrode and suggest an approach suitable for extending the metallic character of the substrate onto the monolayer.

1. Introduction

Despite continuous progress, top-down techniques for structuring at the nanoscale are expected to eventually reach their technological limits. Bottom-up approaches based on the spontaneous self organization of suitable building blocks into well-defined superstructures present an appealing alternative. Self assembly is encountered in many natural systems including liquid crystals, block co-polymers, semiconductor quantum dots, and metal nanoparticles. In particular, small molecules are highly attractive building blocks, as their individual properties, the manner of self assembly into well-ordered supramolecular architectures, and the functionality of these structures can be custom-tailored through the rich chemistry of organic systems.[1] With the advent of nanotechnology, especially the interest in self-assembled molecular (mono)layers on surfaces has steadily increased. Such 2D-crystalline structures can be classified on the basis of the interaction amongst the individual building blocks as well as the interaction between adsorbate and substrate. They comprise, for example, hydrogen bonded systems,[2,3] extended grid-type structures resulting from the assembly of transition metal atoms with suitably chosen ligands,[4,5] quasi-epitaxially growing layers,[6] chemisorbed organic molecules experiencing strong charge transfer to the metal, where long-range order arises from the electrostatic interaction of the charge-transfer dipoles,[7] and strongly (often covalently) bonded layers of essentially upright-standing molecules usually referred to as SAMs (i.e., self-assembled monolayers).[8,9,10,11,12,] As far as the latter are concerned, it is useful to distinguish between SAMs on noble metals,[13,14,15] on semiconductors,[16,17] and on conducting[18,19] or insulating oxides.[20] Here, we focus on the modeling of the properties of SAMs formed by π-conjugated or aromatic molecules strongly bonded as thiolates to noble metal substrates, gold in particular. However, many of the fundamental concepts described below can (with certain adaptations) also be applied to other self-assembled systems on surfaces.

Single (or at least thin) layers of covalently attached organic molecules hold high technological promise[8,12,15] for the modification of a number of macroscopic surface properties.[21,22] In organic thin film transistors (OTFTs), they have been employed to form or modify gate dielectrics,[23,24,25,26,27,28] to shield interfacial trap states allowing for ambipolar transport,[29] to realize new device functionalities,[30,31] as the active semiconductor layer,[30,32,33] and to control growth and morphology of the organic semiconductor.[34,35] Importantly, SAMs have also been utilized to control the rates for charge-carrier injection from metallic

electrodes into organic semiconductors in OTFTs [34,35,36,37] and other organic electronic devices.[38,39,40] For these latter applications, the first relevant electronic interface parameter is the barrier for electron or hole injection, i.e., the energetic separation of the conducting states in the organic semiconductor from the Fermi level (E_F) of the electrodes. Thus, the central topic of this Progress Report will be how SAMs change the work function, Φ, of a metal surface and how the chemical structure of the molecules in the SAM impacts the achievable work-function modification, $\Delta\Phi$. As a further step, we will address under which circumstances this SAM-induced $\Delta\Phi$ directly translates into changes of the charge-carrier injection barriers into an organic-semiconductor layer deposited on top of the SAM (**Figure 1**a)

The second relevant electronic interface parameter is the additional barrier for charge carriers imposed by introducing the SAM, which is defined by the alignment of the frontier electronic states within the SAM relative to E_F. This parameter also establishes the link to another area of research, where the interface energetics of covalently bonded molecules plays a pivotal role, namely molecular electronics. There, the device functionality is directly embedded into monolayers or even into individual molecules and their interfaces with metal electrodes (Figure 1b). [41,42,43,44,45,46,47,48,49,50,51,52,53,54] Therefore, we will also discuss how this interfacial energy-level alignment can be modified by changing the chemical structure of the adsorbed molecules, what limits control over that alignment, and how neutral radicals provide a possibility for overcoming these limitations.

It is conceptually appealing and insightful to abstractly separate a SAM/substrate system into an organic part (the molecular monolayer) and an inorganic part (the metal), and then consider the effect of chemical bonding between these two components. This partitioning also highlights that SAMs not only connect the organic and the inorganic worlds but also lie at the interface between two disciplines of science, chemistry and physics. Furthermore, there are essentially three parts of the SAM-forming molecules that can, within the limits of synthetic chemistry, be modified independently: the docking group that bonds the molecules to the electrode(s), the backbone, and polar or otherwise functional head-group substituents; a number of possible combinations that will be addressed in this report are shown in the bottom part of Figure 1. Following the above mentioned partitioning scheme, we will first highlight some fundamental aspects of free-standing molecular monolayers and then discuss their covalent bonding to a metal substrate. Subsequently, we will elucidate the impact of the

individual components of a SAM listed above on the relevant interfacial electronic parameters, work-function modification and level alignment. The last part of this report focuses on the impact of the molecular packing density on the electronic structure of a SAM.

2. Fundamental aspects regarding the electronic structure of SAMs

Most functional SAM-forming molecules possess a permanent dipole moment. Additionally, charge rearrangements occurring at the metal-SAM interface upon bond formation give rise to a dipole moment. Thus, a first intuitive picture for the interfacial electronic structure in SAMs can be derived from basic electrostatic considerations.[55,56] To quantify insights gained from this picture, i.e., to evaluate work-function changes or energy level alignments and to visualize quantities like the electrostatic potentials, charge densities, or (local) densities of electronic states, quantum-mechanical calculations are useful. Commonly, periodic density-functional theory (DFT) based slab-type calculations are employed.[57,58,59,60,61,62,63] There, a slab consisting of a few atomic layers represents the substrate surface and molecules are typically adsorbed on one side of the slab (**Figure 2**). A lateral unit cell is defined (Figure 2a) which is periodically repeated, thus representing an infinitely extended two-dimensional system. As periodic boundary conditions need to be imposed also in the third direction, *z* (perpendicular to the surface), a vacuum gap needs to be introduced between two consecutive images of the slab in most band-structure codes in order to suppress spurious electronic interactions between the periodic replicas (Figure 2b). For the asymmetric systems discussed in the present Report, i.e., a substrate slab with dipolar molecules adsorbed on only one side, a step in the electrostatic potential is introduced in the vacuum gap to compensate for the net dipole moment of the system in *z*-direction (Figure 2b);[64] this procedure suppresses artificial electric fields which, otherwise, would arise from imposing periodic boundary conditions also in the third dimension.[65] The approach just outlined also permits studying free-standing monolayers, i.e., 2D molecular crystals. The benefit of that will become obvious below. If required for the sake of consistency, also non-periodic systems, e.g., individual molecules can be treated by band-structure codes by placing them into a sufficiently large rectangular "box".

As the typically investigated systems are of a size that renders more exact theoretical methods computationally unfeasible, well-known shortcomings of state-of-the-art (semi)local DFT have to be considered. In particular, the notorious underestimation of transport gaps in semi-

conducting and insulating materials precludes quantitative statements on the energies of the frontier electronic states in the SAM. Nevertheless, even a qualitative discussion thereof reveals important insights on the interfacial electronic structure. While the inherent inability of (semi)local DFT to describe intermolecular van der Waals interaction must be expected to impact, e.g., calculated adsorption energies, the molecular orientation in densely packed SAMs is more robust as it is mostly determined by repulsive forces; e.g., in prototypical molecular crystals, standard DFT reproduces the molecular orientation determined by X-ray diffraction reasonably well.[66]

2.1 Electrostatic properties of molecules and free-standing monolayers

As a first step, it is important to realize the fundamental differences in the "electrostatic properties" of an isolated polar molecule and a quasi-infinitely extended two-dimensional monolayer consisting of polar molecules. The potential energy of an electron (simply given by the negative of the elementary charge times the electrostatic potential) around one individual molecule in vacuum is shown in **Figure 3**a for the example of HS|2P|CN (i.e., a thiol docking group, a biphenyl backbone, and a cyano head group). While a pronounced "bump" is visible adjacent to the –CN group (around which the molecular dipole moment is largely localized), the potential energy assumes a constant value, the vacuum level E_{vac}, already at relatively small distances from the molecule. The molecular ionization potential, IP, and its electron affinity, EA, are unambiguously defined with respect to that reference energy; they reflect the energy balance for removing an electron from or adding an electron to the molecule. These quantities can be tuned, for example, by attaching electron rich (donating) or, as in the case of the cyano group, electron poor (accepting) substituents to the molecular core.

The situation is markedly different for a (hypothetical) free-standing monolayer of infinite lateral extent, which is built up from parallel dipolar molecules.[67] There, as depicted for an ideal HS|2P|CN layer in Figure 3b, the SAM divides space into two regions with distinctly different vacuum levels.[68] To stay consistent with the SAM orientation sketched in Figure 1a, in the following the docking-group side will be referred to as the "left" region and the head-group side as the "right" region. As a consequence of the step in the electron potential energy across a layer of dipolar molecules, the resulting IP and EA depend on whether an electron is removed from or added to the SAM on the right side or the left side. Thus, in such a situation one is always dealing with pairs of quantities, namely a left and a right vacuum level, E_{vac}^{left} and

E_{vac}^{right}, a left an a right ionization potential, IP_{left} and IP_{right}, as well as a left and right electron affinity, EA_{left} and EA_{right}. For a free-standing monolayer of *finite* extent, a single E_{vac} can again be defined, but the electron potential energy around such a SAM reaches this value only at distances significantly larger than the monolayer's lateral extent.[69] Therefore, it is of no consequence for the interfacial energy-level alignment between two materials that are in intimate contact (e.g., an organic semiconductor on top of the SAM), and considerations valid for the model case of infinite lateral extent can safely be applied at least as long as no laterally extended defects exist in the SAM. The role of the latter is discussed in detail, for example, in Ref. [55].

The magnitude of the step in the potential energy across a free-standing SAM (Figure 3b), i.e., the difference between the left- and right-side vacuum energies, ΔE_{vac}, is given by the heuristic Helmholtz equation:

$$\Delta E_{vac} = -\frac{(-e)\mu_{\perp}}{\varepsilon_0 A} = \frac{e\mu_0 \cos(\beta)}{\varepsilon^{eff}\varepsilon_0 A} \qquad (1)$$

Note that, for the sake of convenience and consistency, energies are given for electrons in Eq. 1 as well as in all following equations and in all plots. This is the reason for the factor $-e$ in Eq. 1, with e being the (by definition positive) elementary charge. A is the area per molecule and $\mu_{\perp}$ is the dipole moment perpendicular to the surface associated with each molecule *within* the monolayer. It is related to the absolute value of the dipole moment of a single *isolated* molecule, μ_0, by the orientation of this dipole moment relative to the surface normal, $\cos(\beta)$, and a depolarization factor, ε^{eff} (see below).

In fact, Eq. 1 arises from solving Poisson's equation for a double layer of two laterally homogenous slabs with opposite charge (similar to a plate capacitor), which leads to the question whether the discrete atomistic structure of a SAM needs to be taken into account in basic electrostatic considerations. This question has been elegantly addressed by Natan et al.,[55] who pointed out that the electric field outside a layer of discrete dipoles decays much more rapidly than around an isolated dipole. While this can be inferred by simply comparing Figures 3a and 3b, a more quantitative estimate for the maximal decay length of the electric field outside a 2D array of dipoles with a rectangular unit cell of dimensions a×b is $l_{max} = \max(a/2\pi, b/2\pi)$.[55] Consequently, the potential inhomogeneities due to the discrete molecular

structure decay on a length scale smaller than typical inter-molecular distances and, thus, as long as the monolayer is densely packed, they do not impact how an organic-semiconductor layer on top of the SAM-covered electrode "sees" the SAM. Only in non-ideal SAMs, e.g., when containing large pin-holes, a significant intrusion of the dipole-induced field into the organic-semiconductor layer can be expected,[55] a notion we will return to in the following subsection and also towards the end of this Report.

2.2 Depolarization phenomena in dipolar SAMs

When treating a SAM as an array of polarizable dipolar objects, the mutual interaction of the dipoles has to be taken into account. In the Helmholtz equation (Eq. 1), this is done by introducing the effective parameter ε^{eff}. We emphasize that ε^{eff} must not be confused with the macroscopic dielectric constant of the SAM. While the latter is related to the response of the free-standing monolayer to a homogenous electric field applied across the layer (**Figure 4**a), the former should be seen as an effective quantity that describes the response of each molecule in the SAM to the (inhomogeneous) electric field created by the dipole moments of all neighboring molecules (Figure 4b).[70] More specifically, neighboring polar molecules give rise to an electric field,[71] which depolarizes any one molecule by inducing a dipole moment that counteracts its intrinsic dipole moment, μ_0. Consequently, the dipole moment of each molecule within the SAM is reduced by a factor ε^{eff} compared to μ_0. For a 2D array of polarizable point dipoles, a closed expression for ε^{eff} can be given:[72,73]

$$\varepsilon^{eff}(n) = 1 + \frac{\alpha}{4\pi\varepsilon_0} k n^{3/2} \qquad (2)$$

Here, n denotes the molecular packing density in the SAM, k characterizes details of the packing geometry in the dipole lattice,[71] and α is the polarizability of one isolated molecule in the direction perpendicular to the layer. Indeed, depolarization effects have been observed in several systems, both experimentally[74,75] and theoretically (for SAMs see, for example, Refs. [58],[59], and [76]), and have been described using equations analogous to Eq. 2.[75,58] A more detailed analysis, however, reveals that this equation cannot be directly applied to SAMs;[70] as intermolecular distances are comparable to the lengths of the molecules, the point-dipole approximation no longer holds. The resulting finite-size effects, which in most cases significantly reduce ε^{eff}, can be accounted for either by introducing an effective molecular

polarizability (obtained by fitting experimental or theoretical data[75,58]) or by resorting to a finite-size parameter.[70,77]

Both, the qualitative difference between the macroscopic dielectric constant and ε^{eff} as well as the necessity for including finite-size effects can be neatly understood by examining the associated charge rearrangements in real space (as calculated by DFT).[70] Figure 4d displays the charge rearrangements, $\Delta\rho_{ind}(z)$, induced by applying and external homogenous electric field across the free-standing monolayer as well as the net charge transfer $Q_{ind}(z)$; both quantities are integrated within the *x*,*y*-plane of the monolayer within the unit cell. $Q_{ind}(z)$, defined by Eq. 3, specifies the total amount of charge shifted from a region to the right of a plane at position *z* to the region left of that plane:

$$Q(z) = \int_0^z \Delta\rho(z')dz' \qquad (3)$$

For both high and low packing densities (see section 5 for details), these plots clearly reveal that the molecules are polarized along their entire length, which microscopically is reflected by charge-density fluctuations on the scale of bond lengths throughout the whole molecular backbone. As a net result, charge is transferred from one end of the molecule to the other.[70]

In contrast, Figure 4e displays the charge rearrangements $\Delta\rho_{depol}(z)$ and $Q_{depol}(z)$ that are induced by the field created by the dipolar head-groups of the molecules within the SAM. They are best visualized by subtracting the charge densities associated with two different packing densities. The solid lines correspond to the difference between full coverage, n_0, and half coverage (i.e., at high packing densities), while the dashed lines reflect the depolarization charge rearrangements in the low-coverage regime, i.e., between $n/n_0 = 0.05$ and $n/n_0 = 0.02$. At low coverage, both $\Delta\rho_{depol}(z)$ and $Q_{depol}(z)$ are very similar to the situation found for an externally applied homogenous electric field. This can be understood by the fact that the field created by the surrounding polar molecules penetrates the loosely packed SAM and is close to homogenous at the location of any one particular molecule (Figure 4c). A markedly different pattern emerges for high coverage.[70] While there are still some minor charge-rearrangements along the entire backbone, significant charge transfer is observed only in the vicinity of the dipolar head-group substitutent. This confirms two points made earlier, namely that the molecular dipole moment is localized around the –CN group and that the field created by a

densely packed layer of such dipoles is largely confined to within that layer.[55] As a consequence, only the polar head-group substituent itself and the immediately adjacent part of the molecule get substantially depolarized, which underlines the necessity for including finite-size effects. Finally, the resulting depolarization factor ε^{eff} is plotted as a function of the coverage in Figure 4f;[70] starting from unity, a slightly sub-linear relationship is observed until, for full coverage, a value of $\varepsilon^{eff} \approx 2.5$ is reached in the case of HS|2P|CN.

The effect just explained also indicates that, in a tightly packed SAM, changing the head-group substituent or the docking group only modifies the potential energy at the respective side of the molecule. Therefore, as will be detailed below, it affects only the right- or left-sided quantities, IP_{right} (EA_{right}) or IP_{left} (EA_{left}).[78,79]

2.3 Basic considerations on SAM-substrate bonding

After discussing the properties of free-standing molecular monolayers, the next logical step is to consider the bonding of the SAM to the substrate; as a representative example, we will in the following focus on bonding to Au(111) surfaces. Clearly, the formation of chemical bonds between the molecules in the SAM and the substrate must be reflected by charge-density rearrangements, $\Delta\rho$, at the SAM/substrate interface. More specifically, $\Delta\rho$ is given by[79]

$$\Delta\rho(\vec{r}) = \rho_{SYS}(\vec{r}) - [\rho_{ML}(\vec{r}) + \rho_{Au}(\vec{r})] \qquad (4)$$

where ρ_{SYS} is the charge density of the combined metal/monolayer system, ρ_{ML} refers to the charge density of the free-standing monolayer alone, and ρ_{Au} denotes the charge density of the gold slab alone. As will be shown below, all these quantities are accessible through DFT calculations on the respective (sub)systems. Integrating $\Delta\rho$ in the plane of the surface (the *x*,*y*-plane) over the unit cell again reduces the dimensionality of the problem and yields $\Delta\rho(z)$. As before, the net charge transfer between regions at different *z*-values, e.g., between substrate and SAM, can then be accessed through $Q(z)$ calculated via Eq. 3. Moreover, the change in the electron potential energy, $\Delta E(z)$, due to the interfacial charge-rearrangements, i.e., the difference to the mere sum of the potential wells of clean gold slab and free-standing SAM, can be evaluated by integrating $Q(z)$ over z (with A being the area of the unit cell in the x,y-plane):

$$\Delta E(z) = \frac{e}{A\varepsilon_0}\int_0^z Q(z')dz' \qquad (5)$$

Note that successively employing Eq. 3 and Eq. 5 corresponds to solving Poisson's equation with the source term $\Delta\rho$ and for certain charge distributions yields the Helmholtz equation (cf., Ref. [56]).

2.3.1 Dissociative adsorption of thiols on gold

For the bonding of thiols (-SH) to noble metals, a complication arises regarding the strict partitioning into a molecular and a metallic part in the spirit of Eq. 4. In contrast to other possible docking groups (cf., Figure 1), adsorption proceeds via the *replacement* of a bond (the S–H bond) with an S–Au bond,[80,81] rather than the *formation* of a new bond. An analogous situation is encountered when using protecting groups.[82,83] This leads to the question of what should be taken as ρ_{ML}, the charge density of the free-standing SAM in Eq. 4, the charge density of the –SH terminated SAM, or that of the monolayer with the hydrogen already homolytically cleaved, i.e., the monolayer terminated by a radical –S• species? The latter approach has been pursued, e.g., by Rusu et al.[60,84,85] and Wang et al.[63] when analyzing the bonding-induced dipoles between methylthiolate or similar molecules and Ag(111), Au(111), or Pt(111) surfaces. A different and chemically more intuitive approach is to modify Eq. 4 for the case of thiol adsorption to include the process of hydrogen cleavage:[56,57,78,79]

$$\Delta\rho_{SH}(\vec{r}) = \rho_{SYS}(\vec{r}) - \{[\rho_{ML}(\vec{r}) - \rho_H(\vec{r})] + \rho_{Au}(\vec{r})\} \qquad (6)$$

Here, ρ_H refers to the charge density associated with the layer of H-atoms saturating the docking-group side of the free-standing thiol SAM.[86] As $\Delta\rho$ calculated via Eq. 4 or Eq. 6 describes two distinctly different processes, namely the bond formation between the Au surface and radical –S• species on one hand and, on the other hand, the replacement of S–H bonds with S–Au bonds,[80] also the derived quantities, interfacial charge-transfer *Q(z)* and interfacial potential energy step *ΔE(z)* must differ. While for other docking groups Eq. 4 can be safely applied,[79] we will in the following use $\Delta\rho_{SH}$ according to Eq. 6 for the description of thiol SAMs.[56,57,78,79] To what extent (if at all) the chosen partitioning scheme affects the electronic structure of the interface will be discussed in subsection 2.4.

Finally, to prevent misunderstandings, we recall that the term "thiol" denotes molecules terminated with an –SH group; if deposited at low temperature, these are the predominant species on the cooled surface.[87,88,89] In contrast, the term "thiolate" is commonly used to indicate the molecular species present at the surface at room temperature, reflecting the fact that, there, the S–H bonds are cleaved.[90,91] Note that, as opposed to the –S• termination mentioned above, "thiolate" actually refers to an $–S^-$ species and will in the following be used to denote molecules bonded via a sulfur group even, as will be shown below, when there is actually little evidence for pronounced negative charging of the sulfur on the surface. We emphasize that the dissociative adsorption of thiols is the only pathway considered in the present Report and, therefore, adsorbed molecules are always denoted as thiolate species. Nevertheless, we will allow "thiol SAMs" as shorthand for "SAMs formed by exposing a surface to thiols".

2.3.2 Notes on the atomistic structure of the thiol/gold interface

Prior to describing the actual interfacial electronic structure, it is necessary to provide a brief account of the current knowledge on the atomistic structure of the thiolate/gold interface. This is because the interfacial charge rearrangements induced by thiol adsorption do depend on the details of the geometry of the sulfur/gold interface. As a comprehensive review of the extensive literature on this topic is well beyond the scope of the present Report, only a condensed sketch is given here.

Earlier studies univocally assumed that the sulfur atoms rest in threefold coordinated hollow sites on an otherwise unreconstructed and defect-free Au(111) surface.[8,92,93,94,95,96] Various DFT calculations on such surfaces have refined this picture by identifying a position between the *fcc*-hollow and the bridge position as the most favorable adsorption site,[97,98,99,100] which indicates that the sulfur predominantly binds to two rather than three gold atoms. This structural model has first been put in question by Fenter et al., who proposed that, after hydrogen cleavage, thiolates on the surface pair up to form disulfide species, thus necessitating two distinctly different sulfur adsorption sites;[101,102] other authors independently arrived at the same conclusion.[103,104] However, these findings are in seeming contradiction to both prior[96] and later[61,105] experimental results, which indicate that disulfides adsorb as individual thiolates via rupture of the S-S bonds on the surface. Furthermore, early DFT calculations on defect-free Au(111) surfaces underlined that the dissociated adsorption state

as individual thiolates is indeed energetically favorable over disulfides.[106,107,108,109,110] Only recently, further theoretical studies could partially reconcile these discrepancies by finding that, while at full coverage adsorption as individual thiolates is clearly preferable, dimerization might indeed occur at lower coverage.[111] Adding to the confusion, further experimental evidence has been advanced, which put the sulfur exclusively at the singly coordinated on-top sites of a defect-free Au(111) surface.[112,113]

These persistent inconsistencies among different experiments as well as between experiment and theory eventually led to the notion of more severe reconstructions of the topmost gold layer upon SAM formation. Yu et al. suggested a structure where the sulfur atoms are located at on-top sites but, in contrast to prior studies,[113] on-top of gold ad-atoms, which the authors claimed to occupy *fcc*- and *hcp*-hollow sites themselves.[114] DFT results on this structure diverge in that it was found energetically preferable when neglecting the energy required for extracting gold ad-atoms from the surface[115] and unfavorable when this energy contribution was taken into account.[116] More light onto possible mechanism involving gold surface reconstructions has recently been shed by low-temperature scanning tunneling microscopy (STM) investigations of thiols on pristine Au(111) surfaces that exhibit the characteristic $\sqrt{3}\times23$ herringbone reconstruction.[117,118] There, it has been suggested that, once hydrogens are cleaved to form thiolate species, the latter tend to dimerize through a Au atom that is pulled from the topmost gold layer.[119] This ad-atom (located at a bridge site) is shared between the two sulfurs which, in agreement with prior suggestions, are now located on-top of gold atoms in the remaining top layer. As the buckled gold surface contains one extra atom per 23 atoms (compared to the bulk structure),[117,118] this process progressively lifts the large-scale Au(111) reconstruction.[119] Reassuringly, theory agrees that the proposed structural motif is energetically stable.[116,119] Furthermore, DFT-based molecular dynamics (MD) calculations suggest that gold atoms can also be pulled from the unreconstructed Au(111) surface covered by thiolates, thus creating vacancies in the top layer.[120,121] This not undisputed[122,123,124,125] model further suggests a dynamic equilibrium between sulfur pairs sharing a gold ad-atom and thiolates adsorbed on bridge sites next to vacancies, which not only seems to fit recent experimental data well,[120,121] but has also been found to be energetically stable in independent DFT studies.[126] Notably, these theoretical investigations[120,121] also found that both, ad-atoms and vacancies are, in fact, highly mobile species. However, neither were the periodically repeated lateral unit cells in these calculations large enough, nor was the time scale of the MD simulations long enough to allow statements concerning their long-range diffusion. While a

very recent DFT study stated that refilling the vacancies would be energetically favorable,[127] STM results further suggest that also the ad-atoms diffuse and coalesce into gold islands of mono-atomic height.[128] Importantly, this latter finding points towards the fact that the ad-atoms do not actively participate in the sulfur-gold bonding after all and, thus, that the sulfur-pair/ad-atom structural motif might occur only during the initial stages of SAM formation, but maybe no longer plays a dominant role in a completed and densely packed SAM.

These most recent contributions are in line with the long-standing observation that, upon increasing coverage, SAM formation first leads to the lifting of the √3×23 herringbone reconstruction of pristine Au(111) surfaces and, subsequently, gives rise to the appearance of ad-atom and vacancy islands;[129,130,131,132,133] the latter are often referred to as "etch pits" as it is believed that trace amounts of gold actually get dissolved in ethanolic thiol solutions and,[134,135] indeed, DFT calculations found that the formation of single-atom vacancies in the topmost gold layer is energetically favored by the presence of methylthiolate on the surface.[136,137] In short, appreciable long-range mass transport appears to be part of the assembly process.[138,139,140,141]

To summarize the above collection of unsatisfactorily diverse statements, the precise atomistic structure of the sulfur/gold interface is still a question of ongoing scientific debate. However, a number of statements can be distilled, in particular:

– SAM formation is a highly dynamic process and not only the equilibrium energetics but also the kinetics play an important role. Both depend appreciably on the chemical structure of the thiol. As mentioned above, methythiolate on the surface strongly favors vacancy formation (i.e., the process becomes exothermic),[136,137] while benzenethiolate only lowers the energy cost for removing a gold atom from the first layer.[142] Moreover, both vacancies and ad-atoms are less mobile in SAMs formed from longer alkylthiols (compared to methylthiol)[120,121] and also in the case of benzenethiol.[143] While, during initial stages of SAM formation, dimers linked via sulfur – gold ad-atom – sulfur bridges might still occur for the latter,[144] the size distribution of ad-atom and vacancy islands at full coverage distinctly differs from that found for SAMs of alkythiols.[143]
– Despite quite explicitly voiced criticism,[102,112,114] DFT-based calculations are well capable of determining the energetic order of different structural motifs. However, as simulating the entire process of SAM formation on a length scale of microns and a time scale of hours is unfeasible, only a finite number of local adsorption geometries can be tested. In

particular, the number of ad-atoms or vacancies involved and their approximate position must often be explicitly set prior to running the calculation; similar intuition is needed for the interpretation of experimental data. Nevertheless, simulations of the type discussed in the present Report will continue to make significant contributions towards reconciliation of diverging experimental observations and towards clarification of key details in the mechanism of metal-molecule bonding.

– It is not (yet) clear how the structure of the gold/sulfur interface for any one type of molecule depends in detail on temperature, coverage, preparation conditions (i.e., ultra-high vacuum or solution, annealing, etc.), solvent,[145] and also on whether SAMs are prepared directly from thiols or rather from acetyl-protected thiols.[82,83]

Despite repeated claims, the question remains whether a single structural motif will ever be found that is universally valid for the sulfur/gold interfaces in all thiol SAMs, regardless of the parameters just listed. One of the main challenges for future research will be to determine whether vacancies and/or ad-atoms are actually incorporated in the sulfur-gold bond, or whether they are transient species during SAM formation that later coalesce to ad-atom and vacancy islands. Given these controversies and the lack of data on conjugated SAMs of the type discussed in the present Report, we will, therefore, limit ourselves to unreconstructed and defect-free metal surfaces here; the potential impact of ad-atoms will only briefly be commented on for one exemplary case. This approach also allows for an internally consistent comparison between different docking groups and different metals where, in comparison to thiols on gold, only few experiments have been conducted.

2.3.3 The bond dipole at the SAM/substrate interface

Having discussed some important general aspects regarding the atomistic structure at the SAM/substrate interface, a more detailed view on the interfacial electronic structure can now be given. For the prototypical example of Au|S|2P|H, a biphenylthiolate SAM on Au(111), a 3D representation of the DFT calculated charge-density rearrangements upon replacement of the S–H bonds with S–Au bonds[80] is shown in **Figure 5**a (see also Refs. [57] and [146]); here, we calculate $\Delta\rho_{SH}$ according to Eq. 6. The plane-integrated quantity $\Delta\rho_{SH}(z)$, the corresponding net charge transfer $Q(z)$, and the derived potential energy step $\Delta E(z)$ are shown in Figure 5b. Several important conclusions can be drawn: (i) For a closely-packed SAM, the charge rearrangements are largely localized at the immediate interface, i.e., the sulfur and the

first gold layer; they decay rapidly on the second gold layer and the first aromatic ring. (ii) There is no net long-range charge transfer between metal and molecule; this is clearly visible in the center panel, where *Q(z)* crosses the zero line between gold and sulfur. (iii) Rather than a single dipole layer, the alternating sequence of charge accumulation and depletion corresponds to a series of small dipoles, whose collective action results in a single pronounced step of the electron potential energy across the metal/SAM interface. For the sake of consistency with previous papers, the total magnitude of the potential energy step will be referred to as "bond dipole", BD, in the following. However, it should be kept in mind that BD actually denotes an energy difference. As will be further detailed below, the magnitude and the sign of BD of course depend on the docking group[79] and details of the local adsorption geometry. Note that, in addition to the formation/replacement of chemical bonds, $\Delta\rho$ and, thus, BD also contain the Pauli pushback of the exponentially decaying tail of the electron density "leaking" out of a pristine metal surface into the vacuum.[56,147]

2.4 A Comprehensive picture of the interfacial electronic structure

The stage is now set to assemble the individual components discussed above into a comprehensive framework which enables understanding all electronically relevant interfacial processes that occur on functionalizing a metal surface with a SAM. The pristine metal substrate is characterized by its potential, the Fermi level, E_F, and the corresponding work function, Φ, as shown in **Figure 6** (upper left panel). The DFT-calculated potential well of the free-standing and H-saturated SAM already introduced in Figure 3b HS|2P|CN is shown in the upper right panel of Figure 6 together with the energies of its highest occupied (HOMO) and lowest unoccupied Kohn-Sham orbitals (LUMO); also indicated are the respective left-sided quantities, IP_{left} and EA_{left}, as well as ΔE_{vac}. The charge rearrangements upon SAM adsorption, i.e., on replacing S–H bonds with S–Au bonds,[80] give rise to a potential energy step across the metal SAM interface, BD (upper center panel), which shifts the potential well of the SAM (and with it HOMO and LUMO) relative to E_F.[148,149]

The final situation after metal-molecule bonding is shown in the lower part of Figure 6. The SAM-induced work-function modification, $\Delta\Phi$, is simply the sum of the two potential energy steps, BD and ΔE_{vac}, i.e., the first relevant electronic interface parameter identified in the introduction is given by:[56,78]

$$\Delta\Phi = \mathrm{BD} + \Delta E_{vac} \qquad (7)$$

For the second relevant interfacial parameter, the alignment of the frontier electronic states in the SAM with E_F, it should be noted that, due to interaction with a continuum of states in the metal, the weakly dispersing energy bands in the SAM are broadened and overlap.[150] Therefore, instead of HOMOs and LUMOs, it is more appropriate to refer to the delocalized frontier electronic states in the bonded SAM as highest occupied π-states (HOPS) and lowest unoccupied π-states (LUPS), respectively.[79] These states can be clearly identified in the density of states (DOS) of the entire system projected onto the molecular part (MDOS), shown on the right of the lower panel in Figure 6. Their energetic separation from E_F is given by the initial energy offset of the left-sided quantities prior to SAM bonding, which is modified by BD according to:[78,79]

$$\Delta E_{HOPS} = \Phi - \mathrm{IP}_{\mathrm{left}} + \mathrm{BD} + E_{corr}^{HOMO} \qquad (8.a)$$

$$\Delta E_{LUPS} = \Phi - \mathrm{EA}_{\mathrm{left}} + \mathrm{BD} + E_{corr}^{LUMO} \qquad (8.b)$$

These quantities are indicated in Figure 6 (bottom panel) together with the resulting ionization potential and the electron affinity of the SAM bonded to the metal, $\mathrm{IP_{SAM}}$ and $\mathrm{EA_{SAM}}$. Comparison with the top right panel in Figure 6 may suggest that the latter are identical to the right-sided quantities, $\mathrm{IP_{right}}$ and $\mathrm{EA_{right}}$, at the head-group terminated surface of the free-standing SAM, but it turns out that they differ slightly. That difference is referred to as E_{corr}^{HOMO} and E_{corr}^{LUMO}, respectively.[79] It can be rationalized by the fact that the internal electronic structure of the SAM and, consequently, its energy levels, are slightly modified upon interaction with the metal as a consequence of the interfacial charge rearrangements. For thiols, the resulting correction energies are typically on the order of 0.2 eV.[79]

We now briefly return to the issue of the formation of S–Au bonds from the radical –S• species vs. replacement of S–H bonds with S–Au bonds in the case of thiols, i.e., the determination of $\Delta\rho$ via Eq. 4 as opposed to $\Delta\rho_{SH}$ via Eq. 6. The respective $\Delta\rho$'s reflect two distinctly different chemical processes, involving distinctly different initial chemical structures but the same final structure: the SAM bonded to gold via the sulfur atom with the hydrogen cleaved from the thiol. Consequently, also the corresponding BD values are

different. For example, BD_{SH} = -0.9 eV and $BD_{S\bullet}$ = +0.9 eV in the case of 4'nitro-4-mercaptobiphenyl on Au(111).[146] Despite this seeming ambiguity, introducing a bond dipole helps to understand and predict the interfacial electronic structure of SAMs, as will become apparent in the following sections. It is important to note that all observables of the final SAM/substrate system are invariant to the partitioning chosen to describe the adsorption process; due to the different electron distribution in the –SH and –S• groups, differences in BD are exactly compensated by differences in IP_{left}/EA_{left} and, concomitantly, ΔE_{vac}.[146] Consequently, the relevant electronic interface parameters $\Delta\Phi$ and $\Delta E_{HOPS}/\Delta E_{LUPS}$ remain unaffected. Nevertheless, the partitioning following Eq. 6, i.e., BD_{SH}, is preferable as it permits extracting more insightful information on the actual bonding-induced interfacial processes; therefore, it will be used for thiols throughout the remainder of the manuscript. In contrast, –S• type partitioning reflects the localization of the radical character in the SAM forming molecules and, thus, one obtains BD values that strongly depend on the degree of conjugation in the SAM backbone; e.g., Rusu et al. obtained a vanishing $BD_{S\bullet}$ for methythiolate on Au(111)[84,85] compared to the +0.9 eV found in the case 4'-nitro-4'-mercaptobiphenyl mentioned above. These differences, however, do not actually reflect differences in the metal-sulfur bond but rather differences in the delocalization of the radical species along the backbone.[151]

3. Relationship between the chemical structure of the SAM and the electronic properties of the interface

Knowing the fundamental aspects determining the electronic characteristics of SAMs, in particular Eqs. 7 and 8, it is relatively straightforward to deduce the impact of changing the chemical structure of the SAM/substrate system. In this section, we first focus on the roles played by head-group substituents and docking groups (cf., Figure 1a). At that stage, the backbone is chosen to be biphenyl in order to deal with an aromatic molecule for which the packing at the surface is relatively well known; 4-methyl-4′-mercaptobiphenyl on Au(111) has been shown to pack in a herringbone pattern with two molecules in a rectangular p($\sqrt{3}\times3$) surface unit cell (Figure 2a).[152,153] Subsequently, important aspects connected to the chemical structure of the backbone will be discussed. To conclude this section we will describe the influence of the degree of coupling between the metal and the π-system, and address the role played by the substrate metal.

3.1 Impact of head-group substituents and docking groups

Following the partitioning scheme introduced in Figure 1, we first turn to the impact of head- and docking groups on the SAM interfacial electronic structure, discussing first the free-standing monolayers and then the bonding to the Au(111) substrate. The impact on the potential energy of changing the head-group substituent from a strongly electron donating dimethylamine- in several steps to a strongly electron accepting cyano-group is shown in **Figure 7**a for the free-standing SAM with a HS- docking group. As anticipated,[56,78] only the potential energy landscape at the substituent side of the free-standing and densely packed SAM is modified, which alters IP_{right}, EA_{right}, and ΔE_{vac}; IP_{left} and EA_{left} are virtually unaffected. Considering the identical shapes of the potential energies at the docking-group side (the left side), it is not surprising that also BD is not affected by the choice of the substituent, at least as long as it does not impact the angle of the long molecular axes with respect to the surface normal. As a consequence, changing the head-group substitution can *significantly change the work-function* of the SAM-covered electrode (for the investigated systems listed in **Table 1**, $\Delta\Phi$ values range from -2.43 to +2.62 eV). However, it does *not impact the alignment between the metal and molecular states* (i.e., ΔE_{HOPS} and ΔE_{LUPS} are unchanged).[78] Especially the latter appears somewhat counterintuitive, considering that attaching electron-donating or -accepting substituents to the molecular backbone significantly modifies its *molecular* IP and EA. However, bearing in mind the peculiar electrostatic properties of a dipolar layer compared to that of an isolated molecule (Figure 3), this observation is easily rationalized.

A qualitatively different behavior is observed when changing the docking group from a thiol to, for example, pyridine[154,155,156] or isocyanide:[157,158,159] In the free-standing monolayers, now the "left" (i.e., docking-side) quantities, IP_{left}, EA_{left} and, consequently, ΔE_{vac} are changed, as shown Figure 7b for the case of plain hydrogen termination at the head-group side. Additionally, a different docking chemistry also induces different interfacial charge rearrangements upon bonding, which give rise to a different BD; for example, Gilman et al. describe a subtle-interplay between σ-donation and π-backdonation for hydrogen isocyanide (CNH) and isocyanmethane ($CNCH_3$) on Au(111) surfaces.[160] Indeed, qualitative and quantitative differences are found in the DFT calculations shown in Figure 7c. Thus, it follows from Eqs. 7 and 8 that the choice of the docking group appreciably impacts *both the work-function modification and the level alignment*.[79] Notably, the bonding-induced charge

rearrangements, $\Delta\rho(z)$ according to Eq. 4, extend further onto the biphenyl backbone for the pyridine docking group, which can be attributed (a) to the pinning of the metal Fermi level at the LUPS of the SAM (*vide infra*) and (b) to a more pronounced rehybridization of the HOPS. The latter point is also reflected in new interface states appearing within the molecular HOPS-LUPS gap and a relatively large E_{corr}^{HOMO} (several tenths of an eV).[79] Lastly, we note in passing that replacing the thiol docking group with a selenol (–SeH) does not affect the interfacial electronic parameters (assuming the same local docking geometry at the interface to the gold substrate),[79] while it significantly increases long-range order in the SAM,[161,162,163,164]

To exemplify how the local atomistic structure at the immediate SAM/Au interface can impact the surface electronic structure, we considered SAMs of cyano-, amino- and unsubstituted biphenylthiolate with the sulfurs on-top of gold ad-atoms, which themselves are situated in *fcc*-hollow sites of an otherwise undisturbed Au(111) surface.[114,122,123,124,125] This structure is not to be confused with the situation also described in section 2.3.2 in which sulfur pairs share a gold ad-atom.[120,121] The results for the defect-free and the inverted honeycomb adsorption structures are listed in **Table 2**. The absolute value of BD is considerably reduced for the structure containing ad-atoms. The consequences of that effect are somewhat compensated by the fact that the work function of pristine Au(111) is already reduced by $\Delta\Phi_{ad\text{-}atom} = -0.52$ eV when adding two additional surface Au atoms per p($\sqrt{3}\times3$) unit cell. For the sake of comparability with the corresponding results without ad-atoms, the $\Delta\Phi$ values in Table 2 are thus obtained by modifying Eq. 7 to $\Delta\Phi = \mathrm{BD_{SH}} + \Delta E_{vac} + \Delta\Phi_{ad\text{-}atom}$. As a net-effect, $\Delta\Phi$ is increased for the cyano-substituted SAM, while the magnitude of the work-function reduction is decreased for the unsubstituted and the amino-substituted SAMs. The changes in BD, $\Delta\Phi_{ad\text{-}atom}$, and a somewhat modified value for E_{corr} result in ΔE_{HOPS} being significantly smaller in the presence of ad-atoms. In fact, ΔE_{HOPS} becomes so small that one is very likely in the regime of *Fermi-level pinning*,[165,166,167] a phenomenon that is discussed in more detail below.

To summarize, changing the head-group substituent and/or the docking group provides largely independent handles to tune both, the energy-level alignment at the SAM/substrate interface and the sample work function over a wide range; an overview of what can, in principle, be achieved can be obtained from Table 1. The main experimental challenges in this context are that (i) some of the required molecules might be hard to synthesize and (ii), even more importantly, the tendency to form densely packed and well-ordered monolayers of

upright-standing molecules might be less pronounced for some species, especially those bearing large intrinsic dipole moments. The latter point is underlined by the fact that, compared to what is actually observed in experiment, both simple estimates according to Eq. 1 and full DFT calculations seem to consistently overrate the work-function changes induced by SAMs of strongly polar molecules.[38,40,60,84,85,82,168,169,170,171] In contrast, for well-ordered SAMs prepared in a highly defined environment, DFT reproduces work-function changes to within the experimental accuracy.[61] This calls for the development of alternative design principles for functional molecules that combine large dipole moments with good SAM-forming qualities.

3.2 The role of the molecular backbone – polarizability

At this point the question arises whether the above-described insensitivity of the level alignment to head-group substitutions could be mitigated by changing the nature of the molecular backbone. More polarizable and better conjugated backbones might result in the impact of substituents reaching further along the molecular backbone. Alternatively, a less polarizable backbone could be expected to less efficiently "screen" the effect of head-groups from the thiolate/gold interface. Thus, we studied a series of backbones with systematically varying polarizability (Figure 1). To isolate the impact of this one parameter, the same packing found in biphenyl-based systems was chosen together with a thiol docking group, while varying the head-group from amino- to cyano-substituents.[172]

Rather surprisingly, it is found that changing the backbone from highly polarizable polyenes (B2) over various intermediate cases (Figure 1) to non-conjugated alkyls has no impact whatsoever on the fact that switching from the electron donating to the accepting head-group does not affect the level alignment at the metal/SAM interface; i.e., for each backbone exactly the same ΔE_{HOPS} values are obtained in the –CN and the $–NH_2$ substituted SAMs.[172] What does, however, change with backbone polarizability is the molecular HOMO-LUMO gap. As, according to Figure 6, a modified HOMO energy changes IP_{left}, also ΔE_{HOPS} changes with the backbone according to Eq. 8a. The calculated ΔE_{HOPS} values are shown in **Figure 8**a, where the orbital energies plotted as the *x*-axis have been calculated for the isolated backbones not bearing substituents or docking groups; note that this plot looks virtually identical for cyano- and amino-substituents. As expected, a linear evolution of ΔE_{HOPS} with the HOMO energy is observed for the larger gap molecules, exhibiting a slope close to one. However, as soon as the HOPS approach E_F, this evolution levels off (plateau region in Figure 8a), thus preventing resonance between the conducting states in the metal (i.e., those around E_F) and the delocalized π-system on the molecule.[172] This *Fermi-level pinning* [165,166,167] is a consequence of interfacial charge rearrangements occurring as soon as the tail of the HOPS crosses E_F (schematically shown in Figure 8b):[173] When the IP_{left} of the free-standing SAM gets too small, a significant portion of the occupied molecular DOS would come to lie above E_F, which is not possible in thermodynamic equilibrium. Consequently, electrons flow from the tail of the HOPS feature into the metal. As the HOPS are typically delocalized over the entire molecular backbone, this charge is transferred over a considerable distance in upright-standing SAMs. By virtue of Eq. 1, this means that already a small net amount of charge

transfer gives rise to a sizable potential energy step, which "pushes" the HOPS peak back down below E_F to establish equilibrium. Consequently, further reducing the HOMO energy (and thus IP_{left}) does no longer influence ΔE_{HOPS}. One consequence of this pinnings is that none of the above-described strategies for tuning the interfacial electronic structure in SAMs can be used to establish a situation where the metallic character of the substrate extends onto the organic layer (i.e., where the Fermi level lies right within the HOPS peak). To that aim, a radically different approach is required, as will be discussed in the next subsection.

Prior to that, the impact of changing the backbone on the achieved $\Delta\Phi$ shall be mentioned. For π-donor or acceptor-substituted conjugated molecules, a more conjugated (and, thus, polarizable) backbone naturally results in a larger amount of charge transfer between backbone and substituent and, thus, in a significantly increased dipole moment, μ_0, of the isolated molecule.[172] According to Eq. 1, one might thus expect that also $\Delta\Phi$ increases with backbone polarizability. Nothing like this is, however, observed for the systems investigated here. The only impact of the backbone chemical structure on $\Delta\Phi$ is that it affects the molecular orientation with respect to the surface normal, expressed through the tilt angle β, which enters into Eq. 1 through $\cos(\beta)$ in the enumerator.[172] The reason why increasing the backbone polarizability and, thus, μ_0 does not help in increasing $\Delta\Phi$ is again rooted in the depolarization effects discussed in section 2.2. Although not quite sufficient to capture the complex situation in polar SAMs,[70,174] Eq. 2 presages that an increased polarizability, α, also results in a higher ε^{eff}, which enters Eq. 1 in the denominator. Hence, what is gained by increasing μ_0 is lost through concomitantly increasing depolarization in more polarizable backbones. The latter effect can be huge. For example, the hypothetical work-function change induced by a SAM of amino-substituted polyenes, HS|B2|NH_2 according to Figure 1, would be approximately five times larger than the value in Table 1 assuming the absence of depolarization.[172, 175]

3.3 Doped SAMs – a "radically" new approach

As neither substitution with donor or acceptor head groups, nor changing the molecular backbone, nor choosing a different docking group, nor, as shall be seen below, altering the substrate work function permit bringing either the HOPS or the LUPS into resonance with the metal states around E_F (Figure 8b), a different approach has to be pursued:[173] Taking a step

back, one can actually borrow from the concepts developed for inorganic semiconductors, where ohmic contacts are realized by using degenerately doped semiconductors.[176] Adapting this concept to organic semiconductors leads to, for example, the system shown in Figure 8c. There, one of the two central carbon atoms of a pyrene derivative is replaced either by a boron or a nitrogen atom. Conceptually similar to *p*-type doping, the former removes one electron from the delocalized HOMO (the molecular equivalent to the valence band) and the latter adds an additional electron to the LUMO (*n*-type doping).[173] The resulting molecule is a *neutral radical* with a fully delocalized but only singly occupied highest molecular orbital (SOMO). This significantly changes the energetic situation at the interface, as sketched in Figure 8d: While the fully occupied HOPS (or the empty LUPS) of a closed-shell molecule *cannot* be brought into resonance with E_F because of Fermi-level pinning (Figure 8b), the same mechanism now forces the SOMO of a (neutral) radical to lie at E_F, independent of its energy in the isolated molecule; again, the necessary charge rearrangements only weakly change the occupation of the frontier molecular level.[177] As a result, the metallic character of the substrate now spreads onto the molecule and resonance between the delocalized molecular π-system and the conducting states in the metal around E_F is achieved. Placing such a neutral radical in a single-molecule junction, i.e., contacting it with a metallic lead on either end (as indicated in Figure 8c), gives rise to a continuous transmission channel for ballistic electrons, which efficiently connects the two electrodes (Figure 8e).[173] An ohmic contact is realized, meaning that, in contrast to closed-shell molecules investigated in such setups,[48,52,53,54] (neutral) radicals do not exhibit a conductance gap and high current across the molecular junction can already flow at low bias. In fact, the calculated current-voltage characteristics shown in Figure 8f show that, in the low-bias regime, the current through the neutral radical is about two orders of magnitude higher compared to the undoped molecule.[173] Recent experimental results support the validity of this concept [178] and a number of other experimental observations hint towards the important role played by radicals for charge transport through single molecules and in molecular electronics.[173,179,180,181,182,183,184,185]

3.4 Tuning the electronic coupling between the π-system and metal

Another important issue in the context of the interfacial electronic structure of SAMs is the strength of the electronic coupling between the π-system on the backbone and the electrons in the metal, i.e., the interaction-induced hybridization and broadening of the molecular states.[186] Clearly, if the docking group is directly incorporated into the conjugated molecular backbones

(Figure 1), the electronic coupling must be expected to be relatively strong compared to a scenario where the conjugation is broken between backbone and docking group. One way to achieve this is to introduce short saturated hydrocarbon chains between, e.g., the biphenyl unit and the thiol. In order to maximize the molecular packing density on the surface, these alkyl segments are fully extended in all-trans conformation and, due to their flexibility, they promote long-range order in SAMs.[187,188,189,190,191,192,193] Furthermore, intriguing odd-even effects with the number of methylene (–CH_2–) units in the alkyl spacers have been observed for a number of properties in these highly 2D-crystalline SAMs, both experimentally[194,195,196,197,198,199,200] and in DFT calculations.[201] More importantly, however, increasing the number of methylene spacer units successively suppresses electronic interaction between metal and conjugated molecular core.[201] The situation of the π-system directly coupled to the metal can be compared to a traditional metal/inorganic semiconductor junction. In that sense, the insertion of non-conjugated alkyl segments gradually converts the system to a nanoscopic metal/insulator/semiconductor junction.[201] The two extreme cases of direct coupling (no alkyl spacer) and six methylene spacer units are shown in **Figure 9** for the example of a biphenyl backbone. Around E_F, metal-induced gap states (MIGS)[62,202,203,204,205] are seen in both cases. They extend onto the sulfur and then rapidly decay along the molecule. Also, the first actual peak in the MDOS can be assigned to the HOPS on the biphenyl core in either system. However, the HOPS are clearly separated from the metal in the case of the SAM containing the hexyl spacer (Figure 9b).[201] In the latter case the first continuous electronic states, which extend from the metal over the alkyl segment onto the molecular backbone, are found at significantly higher binding energies. This suggests a considerable energy barrier for hole (and electron) transfer between metal and conjugated core in that system.[201]

3.5 Impact of the substrate metal

Having introduced the bond dipole of aromatic thiols on gold, we now briefly comment on the impact of the substrate metal. While Au(111) is clearly the most commonly used substrate for SAMs, also various crystal faces of silver,[206,207,208,209] copper,[210,211,212,213] palladium,[214,215,216] and platinum[206,217,218,219] have been experimentally investigated. Also (liquid) mercury has been used.[220,221] Due to differences in their lattice constants and their chemical nature, also different packing motifs and/or different surface reconstructions might be encountered on these substrates. Indeed, several possibilities have been proposed for SAMs of short-chain

alkylthiols both from experiments[222,223,224] and from theory.[60,115,225,226] In contrast, little is known about the packing and the atomistic structure of the docking-group/substrate interface for conjugated SAMs, which are the focus of the present Report; it appears unreasonable, however, to simply assume the $\sqrt{3}\times\sqrt{3}$ commensurability of S-atoms found on Au(111) also in calculation of SAMs on, for example, Cu(111),[227] due to the significantly smaller lattice constant of the latter. Consequently, the following comparison is restricted to Ag, which has essentially the same lattice constant as gold. For the sake of consistency, a defect-free (111) surface and a herringbone packing of the biphenyl backbones is assumed also here. In fact, the main structural difference between thiol SAMs on the two metals appears to be that the first sulfur-carbon bond on the molecular side of the interface is slightly less inclined to the surface normal on Ag than it is on Au.[197,198,199,200,201,228,229]

In terms of the interfacial electronic structure, the most relevant difference between silver and gold is the work function ($\Phi_{Au(111)} \approx 5.3$ eV and $\Phi_{Ag(111)} \approx 4.7$ eV).[230] In particular, Eqs. 8 suggest that changing the work-function of the metal might impact the alignment of its Fermi level with the HOPS and LUPS in the SAM. Interestingly, this is not the case. For densely packed SAMs, ΔE_{HOPS} and ΔE_{LUPS} are found to be virtually identical on both metals.[56,79,186] Reexamining Eqs. 8 leads to the conclusion that, if neither the level alignment nor the quantities of the isolated SAM (IE_{left} and EA_{left}) change, the difference in the substrate work function must be compensated by a difference in BD, and this is indeed observed.[56,79,186] Translating this observation to the SAM-induced work-function modification via Eq. 7 yields the equally intriguing result that, despite the considerable difference in Φ of the pristine metal surfaces, the work functions of the SAM-covered surfaces are nearly identical.[56,79,186] These peculiarities regarding level alignment and $\Delta\Phi$ are in agreement with experimental[38,40,231] and independent theoretical results.[84]

4. Organic semiconductors on SAMs

Focusing on the application of SAMs in organic electronics, we now address how the interfacial electronic structure evolves when depositing an organic semiconductor on top of a SAM (cf. Figure 1a). This requires modeling the complete three-component system, which has first been done on the basis of the unified induced density of interface states model by Betti et al.[232]

The main question in that context is to what extent changes of the electrode work function (induced by the SAM) actually translate into changes of electron- or hole-injection barriers into a subsequently deposited organic semiconductor (OSC).[233] A schematic of the investigated structure is shown in **Figure 10**a. To span a wide range of work functions, all the SAMs with biphenyl backbones from Table 1 have been studied and, as OSC, a single layer of biphenyl (2P) was chosen because epitaxial growth on the SAMs is realistic for this material. Considering the well known fact that DFT severely underestimates band-gaps[234] and that the band gap of oligo(phenylene)s decreases with increasing number of phenyl rings,[235, 236,237] 2P actually serves as a model for oligo(phenylene)s with a larger number of repeat units.

The resulting separations of the HOPS and LUPS peaks of the biphenyl OSC layer from the Fermi energy ($E_{LUPS}^{2P} - E_F$ and $E_F - E_{HOPS}^{2P}$) are plotted in Figure 10b as a function of the work-function of the SAM-modified Au(111) electrode, Φ_{mod}. The former quantities are related to the hole- and electron-injection barriers, albeit these are typically defined as the distance between the Fermi energy and the HOPS and LUPS onsets.[238,239] Such a definition would, however, not be particularly useful for analyzing the output of DFT calculations, as the peak widths are affected by methodological details.[233, 240] In analogy to inorganic metal/semiconductor junctions[204, 241 , 242 , 243] and to non-covalently bonded metal/OSC junctions,[165,166,167,238,244,245] a slope parameter can be defined as:

$$S = -\frac{d(E_F - E_{HOPS}^{2P})}{d\phi_{\mathrm{mod}}} \qquad (6)$$

Over a relatively wide work-function range (i.e., for Φ_{mod} between ca. 2 eV and 5 eV), S equals unity and the SAM-induced work-function change directly translates into a change of the injection barriers. A detailed analysis[233] shows that in this region vacuum level alignment occurs between the SAM and the OSC, i.e., no additional interface dipole is formed at the SAM/OSC interface and the work-function of the SAM-covered metal does not change any further upon addition of the 2P layer ($\Delta\Phi_{2P}$ = 0); strictly speaking, fully symmetric Pauli push-back at the organic/organic interface (left panel in Figure 10c) is observed only for hydrogen-terminates SAMs, but also for the other systems $\Delta\Phi_{2P}$ remains below ~0.2 eV.[233] Note that this situation is markedly different from directly depositing OSCs onto pristine metal surfaces, where one observes significant Pauli push-back (of the order of several tenths of an eV);[147]

For Φ_{mod} smaller than ~2 eV or larger than ~5 eV the slope parameter becomes zero. In those regions, the excess work-function modification has no more impact on the injection barriers. The reason is again Fermi-level pinning; only this time, E_F is pinned at the HOPS or LUPS of the additional 2P layer.[233] The pinning manifests itself in an extra work-function change induced by the 2P layer that linearly depends on the excess modification of the sample work function, with $\Delta\Phi_{2P}$ being positive for Φ_{mod} < ~2 eV and negative for Φ_{mod} > ~5 eV. Notably, $\Delta\Phi_{2P}$ vanishes when removing the metal substrate in the calculations, i.e., when studying only the free-standing SAM/2P double layer.[233,246] This underlines the crucial importance of the metal being present for the evolution depicted in Figure 10b.

Consequently, one might expect charge transfer between the metal and the OSC to be responsible for the observed pinning. Nothing like this, however, happens, as is shown in the right panel of Figure 10c for the situation with the smallest Φ_{mod}. On the metal, there is virtually no charge-density rearrangement, $\Delta\rho(z)$, which is defined here as the plane-averaged charge-density difference between the complete system and the non-interacting SAM-covered metal and 2P layer, respectively. Instead, electrons are transferred from the upper (i.e., right) region of the SAM to the lower (i.e., left) region of the 2P layer and, additionally, the SAM backbone is polarized without significant long-range charge transfer along the backbone. These findings are best visible in the plot of the integrated net charge transfer $Q(z)$ as defined in Eq. 3.

Interestingly, for certain ranges of metal work-functions, similar pinning situations have also been observed experimentally in situations where an OSC was separated from the conducting substrate by an insulating layer or another relatively thick semiconductor layer.[165,166,247,248] These observations have been explained by an integer charge transfer between the conducting electrode and the organic semiconductor. The pinning distance (i.e., the energy difference between the HOPS peak of the semiconductor layer and the Fermi level at which pinning occurs) in these experiments was typically larger than in the situation discussed above. This can be explained by charges in the above considered perfectly ordered, crystalline, and defect-free organic semiconductor layer being more delocalized, as discussed in more detail in Ref. [233].

5. Impact of molecular packing density

Having addressed the fundamental properties of perfectly ordered and densely packed SAMs of well-aligned molecules, it is necessary to also discuss the consequences of non-ideal situations. This is particularly important, as in many (presumably the vast majority of) experiments the actually encountered SAMs deviate from the ideal situation assumed in the present Report so far. In fact, to the best of our knowledge, no experimental study on a conjugated SAM has been published, in which the authors have pinpointed the structure and order of the SAM, e.g., by combining diffraction and scanning-probe techniques and, on the same sample, measured the electronic properties, e.g. by photoelectron spectroscopy. Assessing the role of SAM imperfections is no minor challenge for modeling either. A full first-principles description would require huge and, therefore, computationally inaccessible super cells as well as dynamical approaches to geometry optimization (as discussed in section 2, defects in SAMs, such as vacancies or ad-atoms, are very likely not static objects). Alternatively, molecular dynamics approaches relying on (semi)empirical force fields[249,250,251,252] combined with quantum-mechanical calculations on selected motifs hold a certain promise to provide additional insight.[253,59] Such approaches would also be required to asses the role of dynamic disorder on, e.g., the work-function modification; there, as reported in sub-section 3.2, the orientation of the molecular dipole moment is of critical importance and, as the orientation of elongated molecules in a SAM is a rather "soft" degree of freedom, spatial and temporal fluctuations of the work function must therefore be expected.

Here, we will discuss only one fundamental aspect, namely the impact of the SAM packing density on the electronic interface parameters $\Delta\Phi$ and ΔE_{HOPS}. While, in densely packed SAMs at full coverage, molecules are usually standing with their long molecular axes close to the surface normal, so called "lying-down" phases are often observed at lower coverage, e.g., for alkanethiols[13,104,129,130,132,140,141] but also for the biphenylthiols.[152,153] In order to isolate the impact of packing density from that of the molecular orientation (which, however, needs to be assessed in future studies in the light of what has been discussed in the previous paragraph), we adopt the following approach:[148,172] First, one of the two molecules in the p($\sqrt{3}\times3$) unit cell is removed from the fully geometry-optimized structure at full coverage, n_0, to achieve a packing density of $n/n_0 = {}^1/_2$. Subsequently, the lateral unit cell is repeatedly doubled along both the *x*- and the *y*-direction. Keeping only one molecule in the resulting super cells, coverages down to $n/n_0 = {}^1/_{16}$ are realized. As the computational cost for such large systems rapidly becomes prohibitive, a still lower coverage of $n/n_0 = {}^1/_{64}$ was calculated only for the

free-standing "monolayer", which actually served as the reference case of non-interacting molecules. At all coverages, the (upright-standing) geometry of the molecule is always kept fixed to the optimized structure at full coverage.

Adhering to the partitioning scheme used throughout this Report, the properties of the free-standing molecular monolayers, $IE_{left/right}$, $EA_{left/right}$, and ΔE_{vac}, are discussed first and, thereafter, the quantities characterizing the bonding to the metal (BD) as well as the full metal/SAM system, ΔE_{HOPS} and $\Delta\Phi$, will be analyzed. More specifically, we will limit ourselves to the prototypical systems of biphenylthiol with amino and cyano head-group substituents.[148] As already apparent from Figures 3 and 4, reducing the coverage in the free-standing SAM must be expected to significantly impact ΔE_{vac} and, thus, IP_{left} and EA_{left}: Firstly, upon decreasing coverage, there must be a continuous transition from the situation depicted in Figure 3b to that in Figure 3a, i.e., $\Delta E_{vac} \rightarrow 0$ for $n/n_0 \rightarrow 0$. From Eq. 1, one could expect a linear decay of ΔE_{vac}, because the coverage decreases and, therefore, the area A per molecule increases. However, as expressed in Eq. 4, also the depolarization factor ε^{eff} depends on the packing density (Figure 4f),[58,70,77,174] resulting in an overall nonlinear decrease of ΔE_{vac}, as shown in **Figure 11**a for both head-group substituents.[148] The natural consequence of this evolution is that the left- and right-sided ionization potentials (Figure 11b) and electron affinities (not shown) approach the same respective values for $n/n_0 \rightarrow 0$, i.e., those of the isolated molecules which, of course, are different for donor- and acceptor-substituted species. Reexamining Figure 4c we recall that, at lower coverage, the electric field generated by the polar head groups starts to penetrate the molecular monolayer,[148] i.e., the left and right sides of the free-standing SAM start to "see" each other. Consequently, IP_{left} and EA_{left} are no longer insensitive to head-group substitutions on the right side whereas, at full coverage, only IP_{right} and EA_{right} are affected (Figure 7).

Turning now to the metal/molecule bonding, also the charge rearrangement at the interface can be expected to depend on the coverage. Moreover, BD, like the molecular dipole, is subject to depolarization effects and at reduced coverages the electron cloud tailing out into the vacuum above pristine metal surfaces is now "pushed back" in to the metal only locally. On the other hand, also the different energy offsets between E_F and IP_{left}/EA_{left} prior to bond formation should influence the details of the bonding-induced charge rearrangements; for the latter reason, BD is also no longer insensitive to the head-group substitution. Together, this

results in a pronounced non-linear dependence of the respective BD values on coverage (shown in Figure 11c).[148]

After having established that the relevant quantities, IP_{left}/EA_{left}, ΔE_{vac}, and BD all exhibit a complex dependence on packing density and, furthermore, that they depend on the head-group substituent for all coverages smaller than $n/n_0 = 1$, it comes as no surprise that the same is true also for the derived quantities, $\Delta\Phi$ and ΔE_{HOPS}. Regarding the work-function modification (Figure 11a),[148] it is interesting to note that, in the case of the cyano-substituted biphenylthiol SAM, the individual nonlinearities of BD(n) and $\Delta E_{vac}(n)$ partially cancel, as they are of opposite sign. This leads to an almost linear increase of $\Delta\Phi$, albeit with a strongly reduced slope compared to what would be expected from naively employing Eq. 1. Conversely, for the amino-substituted SAM, ΔE_{vac} and BD have the same (negative) sign, which results in a pronounced sub-linear decrease of the sample work function with increasing coverage. We note that similar theoretical investigations regarding $\Delta\Phi$ have independently been performed for SAMs of (fluorinated) alkanethiols on gold[60,85,170] and substituted benzenes on silicon.[58]

Finally, as expected, also the level alignment (shown for ΔE_{HOPS} in Figure 11d)[148] exhibits a pronounced nonlinear dependence on packing density and, furthermore, it turns out to be independent of the head-group substitution only at full coverage. In contrast, at low-coverage, ΔE_{HOPS} in the amino case is lower by as much as 0.5 eV compared to the cyano-substituted SAM. Especially the coverage dependence bears important consequences for comparing different experiments (or calculations) in the field of molecular electronics: As the level alignment critically impacts the current through a molecular wire,[173] appreciable differences must be expected [63, 254 , 255] between molecules embedded in a densely packed SAM [43,44,45,47,48,49,50] and isolated species contacted individually by two metal electrodes.[48,52,53,54]

6. Conclusions

Significant insight into the interfacial electronic structure of self-assembled monolayers on noble metals can already be gained from purely electrostatic considerations. Further and more fundamental understanding is obtained from quantum-mechanical modeling, which usually relies on slab-type band-structure calculations on the basis of density functional theory. Here,

it is shown how a detailed microscopic picture of the relationship between the chemical structure of the molecules and the electronic properties of the SAM-covered metal can be developed. This done by first understanding the properties of isolated monomolecular layers and then combining that with knowledge on the interfacial charge rearrangements upon subsequent bond formation. In this context, it is explained why end-group substituents allow changing the work function but do not affect the level alignment between SAM states and the metal Fermi level. We describe why changing the docking group affects both quantities and compare gold and silver substrates. Fermi-level pinning for small-gap molecular backbones is observed and it is demonstrated that increasing the molecular dipole moments through more polarizable molecular backbones does not impact the achievable work-function change. We also suggest that neutral radicals allow establishing Ohmic contacts between metal substrates and organic layers. Furthermore, it is discussed how the interaction between the π-system of the SAM and the metal can be tuned through aliphatic linkers, and to what extent SAM-induced work-function modifications directly translate into a change in the barriers for electron- and hole-injection into organic semiconductor layers deposited on top of the SAM. Lastly, we elucidate the complex dependence of all relevant interfacial electronic parameters on the packing density of molecules on the surface.

Acknowledgements

The authors would like to thank L. Romaner, G. M. Rangger, O. T. Hofmann, A. Track, A. Natan, L. J. Wang, Z. Shuai, and J. L. Brédas for their invaluable contributions to this work. Financial support by the Austrian Science Fund through project E-1513P20972 and by the DFG through Sfb 448 is gratefully acknowledged.

Received: ((will be filled in by the editorial staff))
Revised: ((will be filled in by the editorial staff))
Published online: ((will be filled in by the editorial staff))

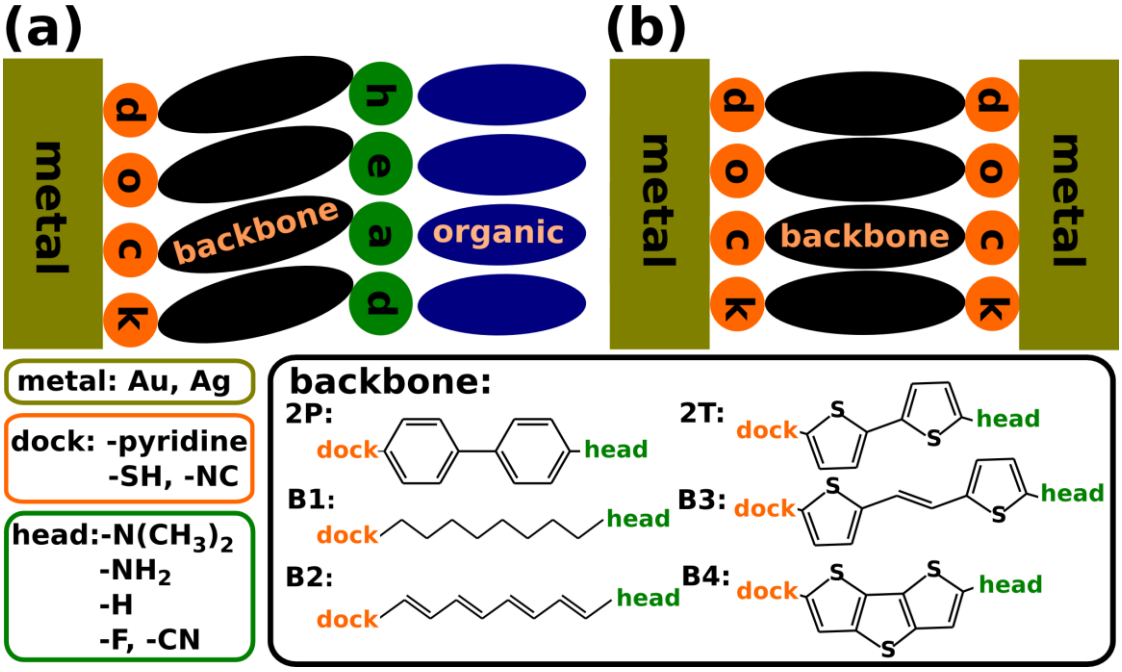

Figure 1. Schematic representation of metal|SAM|OSC heterojunctions (a) and metal|SAM|metal contacts (b). The self assembled monolayer can be understood as consisting of three parts: the docking groups, through which they are bonded to the metal, the rod-like, typically π-conjugated backbone, and the head group, which can be an electron donating/accepting polar substituent. The systems discussed in this study are listed in the bottom part of the figure. The nomenclature used for SAMs throughout this Report is (metal|)docking group|backbone|head group.

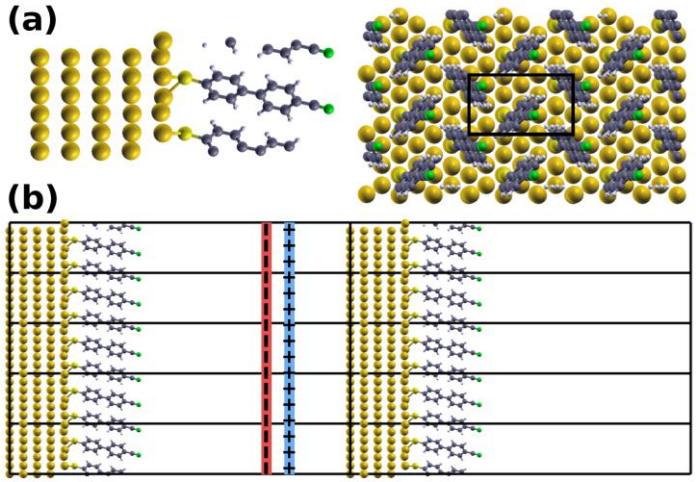

Figure 2. (a) Left: Side view of a typical unit cell containing two molecules on a Au(111) surface. Right: Top view of a larger region. The unit cell is marked by a black rectangle. (b) Illustration of the periodicity of the unit cell. A vacuum gap between neighboring slabs prevents spurious quantum mechanical interaction and a dipole layer is placed in the vacuum to prevent electrostatic interaction between the slabs.

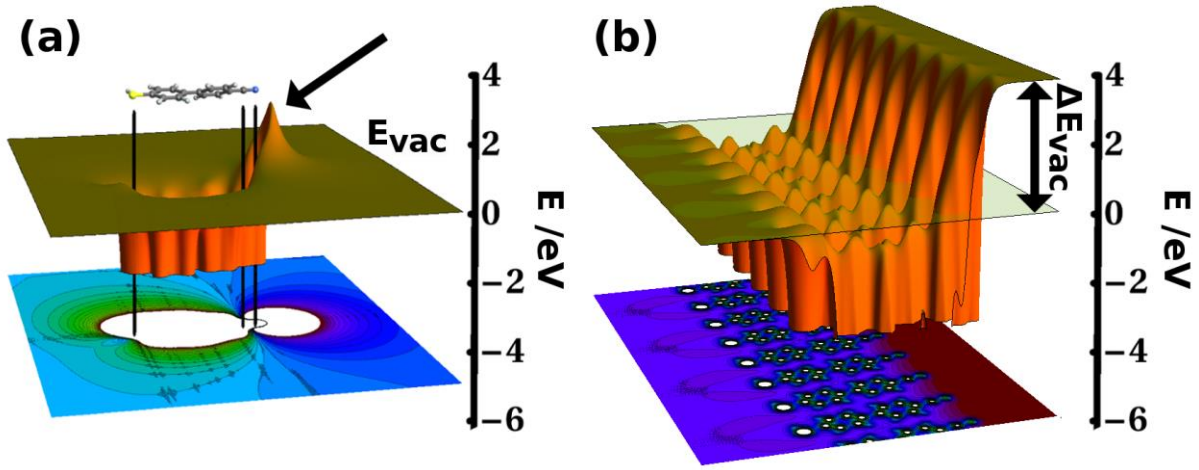

Figure 3. (a) Electron potential energy in the plane of an isolated HS|2P|CN molecule and corresponding contour plot. The black vertical lines help locating the position of docking and head group in both plots. (b) Equivalent plots for an infinitely extended two-dimensional HS|2P|CN SAM, averaged over one dimension. A transparent plane at the energy of the left side vacuum level helps spotting the step ΔE_{vac} in the electron potential energy across the monolayer.

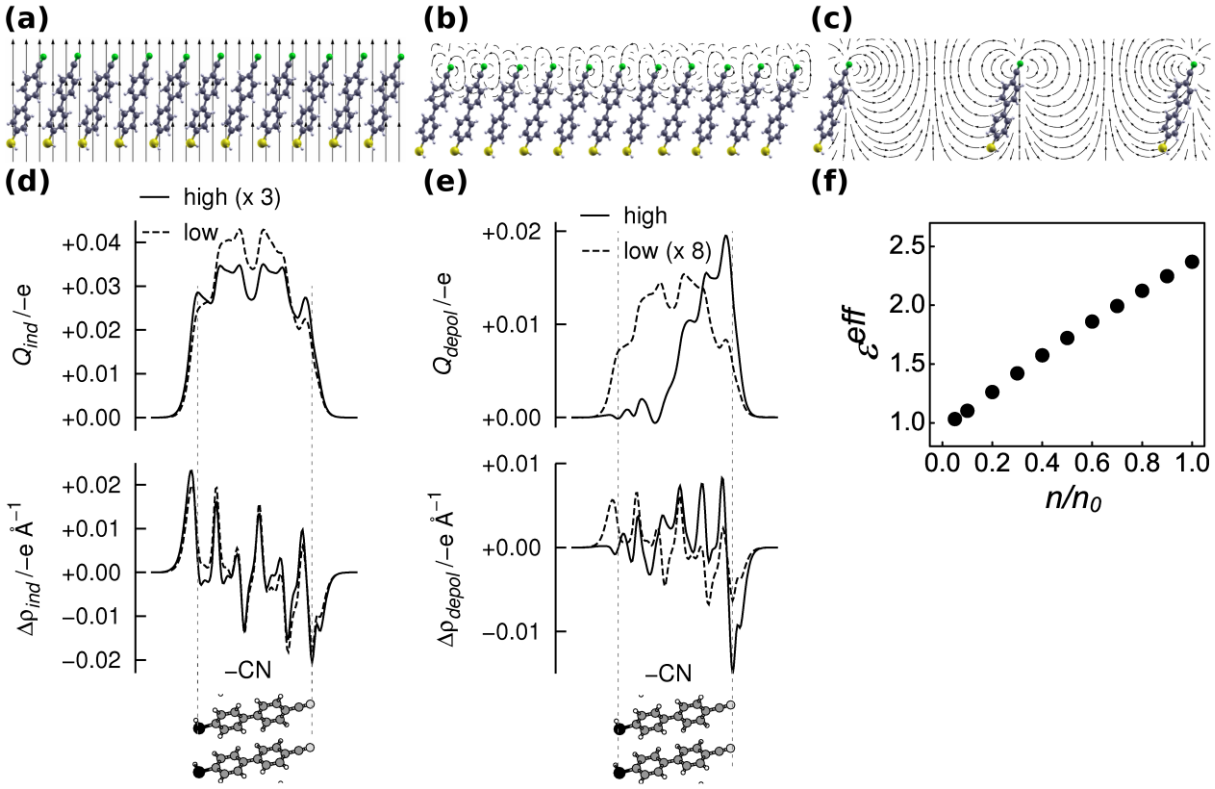

Figure 4. (a): Hypothetical free-standing monolayer exposed to an external, homogenous electric field. (b) and (c): Schematic representation of the electric fields generated by the head-groups in a densely (b) and a loosely (c) packed HS|2P|CN SAM (depolarization effects are not considered). (d): Charge rearrangements $\Delta\rho_{ind}(z)$ and net charge transfer $Q_{ind}(z)$ for the HS|2P|CN SAM upon switching on a homogenous external field of magnitude 0.1V Å^{-1} in the direction indicated in panel (a). The solid lines refer to high coverage (n/n_0=1, multiplied by a factor of 3) and the dashed lines to low coverage, n/n_0=0.02. (e) Depolarization charge rearrangements $\Delta\rho_{depod}(z)$ and $Q_{depol}(z)$ for low coverage (dashed lines; difference between n/n_0=0.05 and n/n_0=0.02, multiplied by a factor of 8) and high coverage (solid lines; difference between n/n_0=1 and n/n_0=0.5). (f) Depolarization factor ε^{eff} as a function of the coverage n/n_0 for HS|2P|CN.

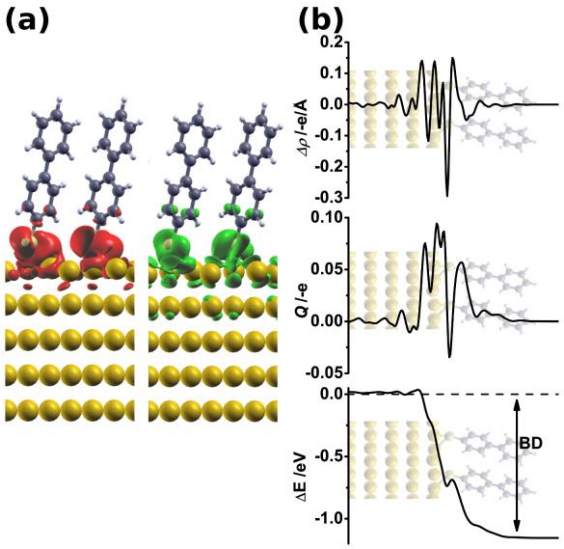

Figure 5. (a) 3-dimensional charge rearrangements $\Delta\rho$ upon bond formation for Au|S|2P|H. The dark gray clouds depicted in the left panel indicate regions of accumulation of electron density, light gray clouds (right panel) mark regions of electron density depletion. (b) Plane-integrated values of $\Delta\rho$ as depicted in (a), charge transfer *Q(z)* and corresponding change in the electron electrostatic energy *ΔE(z)* (details see text). The resulting bond dipole is indicated. The illustrations in the background serve as guides to the eye.

Adapted with permission from ref. [79]. Copyright 2007 American Chemical Society.

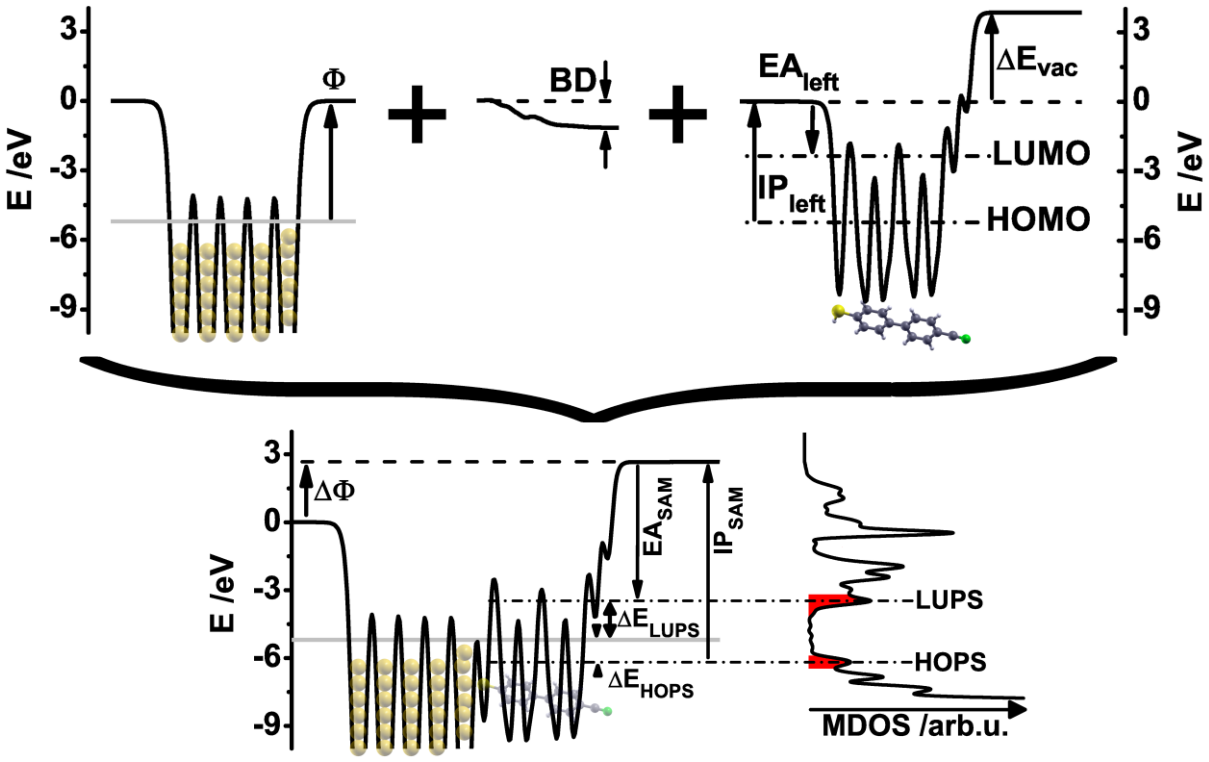

Figure 6. Bond formation and electronic structure of the metal/SAM interface. The plane averaged electron potential energy of the combined system (lower panel) results from the potential energy landscapes of the isolated metal (upper left panel) and SAM (upper right panel) parts, modified by the impact of the bonding as given by the BD (upper central panel). Relevant left- and right-sided quantities are also shown; the Fermi energy is indicated as light gray line. The density of states projected onto the molecular region after bonding is depicted at the right sides of the lower panel. The areas of the HOPS and LUPS peaks are shaded in dark gray.

Adapted with permission from ref. [56]. Copyright 2008 American Chemical Society.

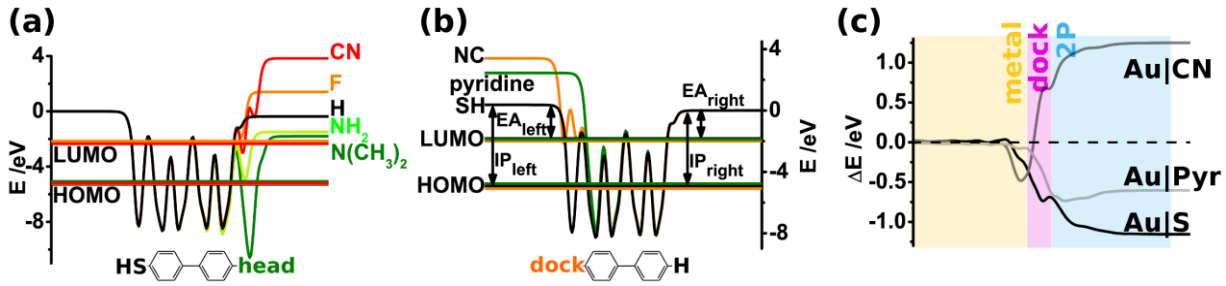

Figure 7. Impact of choice of the head group (a) and the docking group (b) on the electrostatic energy landscape for biphenyl-based SAMs. Left- and right- quantities are depicted in panel (b) for HS|2P|H and schematic structures serve as guides to the eye. (c) Change in the electron potential energy resulting from the charge rearrangements for three docking groups on Au(111): isocyanide (Au|CN), pyridine (Au|Pyr) and thiolate (Au|S).

Adapted with permission from ref. [79]. Copyright 2007 American Chemical Society.

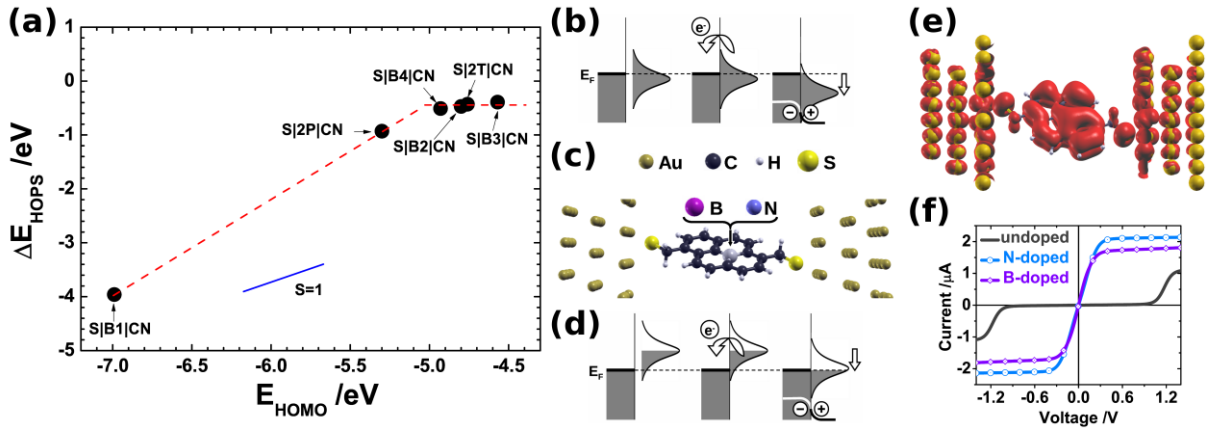

Figure 8. (a) Energetic distance between the highest occupied delocalized states in the SAM and the Fermi level, ΔE_{HOPS} as a function of the highest occupied delocalized molecular orbital of the isolated backbone, E_{HOMO}, for the backbones listed in Fig. 1. (b) Fermi level pining at metal/closed shell molecule interfaces. From left to right: If the highest occupied orbital (HOMO) approaches E_F, charge is transferred to the metal to prevent occupied states above E_F. As a consequence, the resulting dipole layer causes a step in the electrostatic potential across the interface, shifting the states down in energy. (c) Geometry of a N- and B-doped pyrene derivative in the metal/SAM/metal junction. (d) Fermi level pining at metal/monoradical interfaces. In contrast to what is shown in (b), the highest occupied orbital is only singly occupied (SOMO) here. Charge transfer then leads to resonance of the SOMO with E_F. (e) Isodensity plot around E_F for the B-doped molecules in the molecular junction representing the transport channel at low bias. SOMO derived states are delocalized over the whole junction. (f) Current-voltage characteristics of the undoped, N-, and B-doped molecule in the junction.

(a) Adapted with permission from ref. [172]. Copyright 2009 WILEY-VCH Verlag GmbH & Co. KGaA, Weinheim
(b) (b)-(f): Reprinted in part with permission from ref. [173]. Copyright 2009 American Chemical Society.

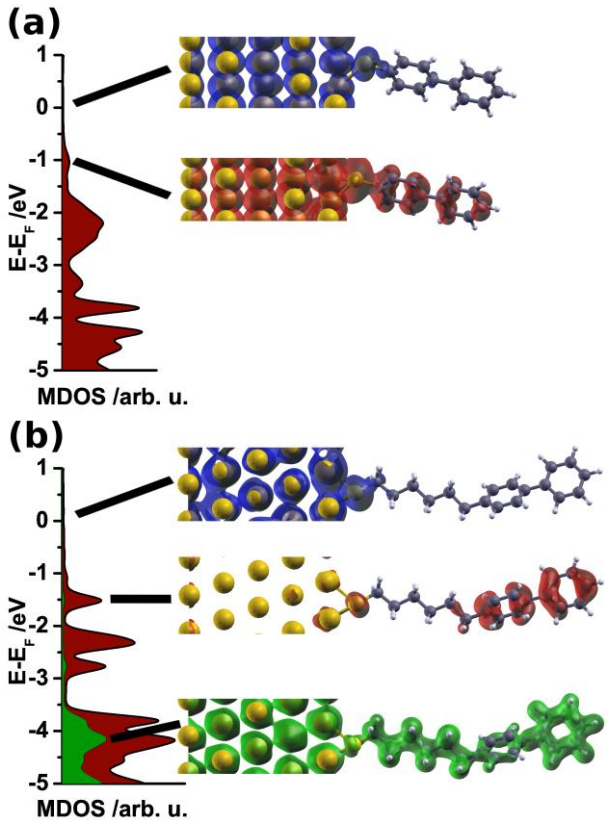

Figure 9. (a): Molecular density of states (MDOS) for Au|S|2P|H (left panel) and isodensity plots of the local density of states for two energy windows. They show metal induced gap states (MIGS) around the Fermi energy (blue clouds) and the delocalized density of states in the HOPS region (red clouds). (b): Molecular density of states when six methylene spacer units separate the π-system and the metal. The orange portion depicts the MDOS only in the alkyl region and the green area the complete MDOS; isodensity plots of the local density of states for the indicated energies showing again the MIGS (top picture), the π-states (central picture) and the fully extended density of states (bottom picture) at energies far below E_F (respectively, at high binding energies).

Adapted with permission from ref. [201]. Copyright 2007 American Chemical Society

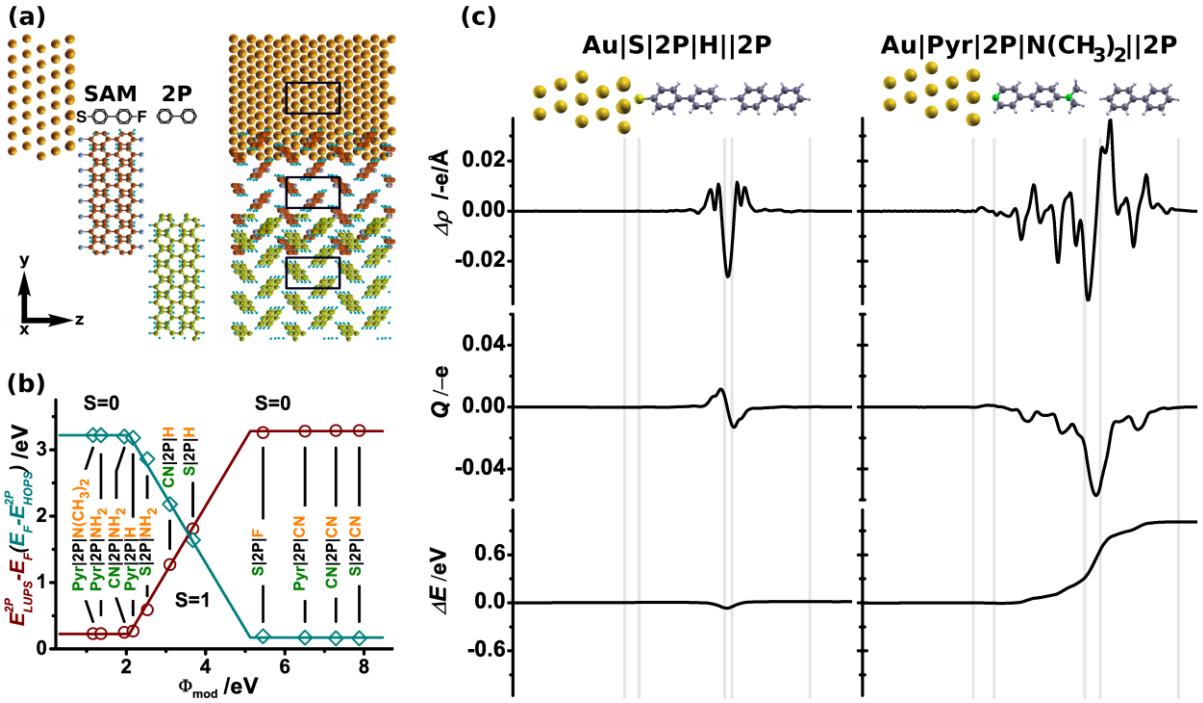

Figure 10. (a): Side and top view of the representative system Au|S|2P|F||2P. The two monolayers (S|2P|F and 2P) are shifted for the sake of clarity. The black rectangles mark the p($3\times\sqrt{3}$) surface unit cell. (b) E_{LUPS}^{2P} -E_F (red circles) and E_F- E_{HOPS}^{2P} (cyan diamonds) as a function of the work function of the SAM covered Au(111) electrode, Φ_{mod}. For the definition of the slope parameter *S*, see text. The values of E_{LUPS}^{2P} and E_{HOPS}^{2P} correspond to the peak positions in the respective molecular DOS (MDOS). The lines serve as guides to the eye. (c) Plane-integrated charge rearrangements upon addition of 2P to the metal/SAM system, $\Delta\rho$, per unit cell (topmost panels), cumulative charge transfer along the *z*-axis per unit cell, *Q*, (middle panels) and change in the potential energy of an electron, ΔE, upon addition of 2P to the system (bottom panels) for two systems. $\Delta\rho>0$ indicates an increase of the electron density, $\Delta\rho<0$ a decrease. Vertical lines and schematic pictures of the systems serve as guides to the eye.

Reproduced with permission from ref. [233]. 2009 American Chemical Society

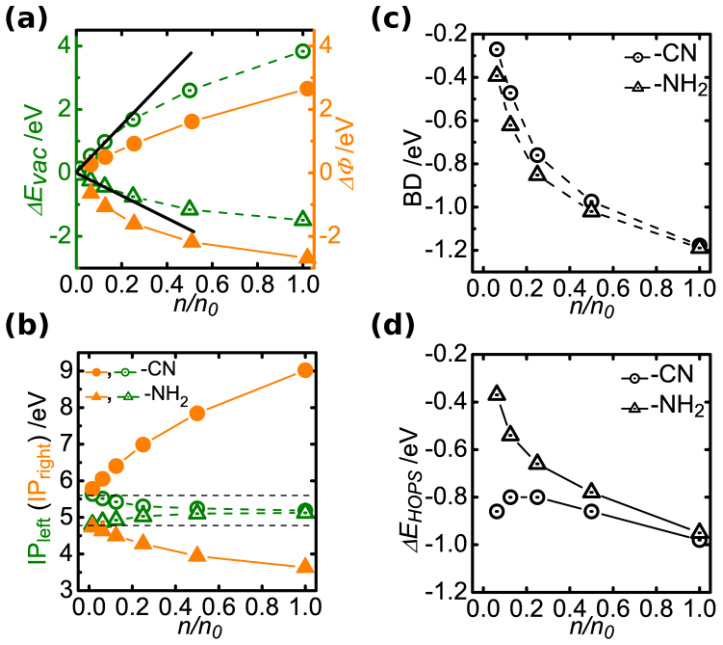

Figure 11. Various SAM properties plotted as a function of coverage n/n_0. Throughout the figure, circles mark the cyano- and triangles the amino-substituted bithenylthiol SAM: (a) step in the electron potential energy ΔE_{vac} (open dark gray symbols) and resulting work-function modification $\Delta\Phi$ (closed light gray symbols), (b) left (dark gray, dotted symbols) and right (light gray, filled symbols) ionization potentials, (c) bond dipole (BD) upon adsorption of the monolayers on Au(111) and (d) distance between the Fermi energy and the HOPS in the metal/SAM systems, ΔE_{HOPS}.

Adapted with permission from ref. [148]. Copyright 2008 American Physical Society

Table 1. Electronic properties of a variety of SAMs on Au(111). ΔE_{HOPS} refers to the alignment of the highest occupied states delocalized over the backbone (HOPS) and the metal Fermi level; IP_{SAM} is the ionization potential of the SAM defined as the energetic difference between the HOPS peak and the vacuum level above the SAM; $\Delta\Phi$ is the SAM-induced work-function modification. Data reproduced from ref. [172] (marked with a '#'), where a sophisticated geometry optimization strategy based on internal coordinates was used. For systems not investigated in that study, data as used in ref. [233] (marked with a '*') is listed.

Systems	ΔE_{HOPS} [eV]	IP_{SAM} [eV]	$\Delta\Phi$ [eV]
Au|Pyr|2P|$N(CH_3)_2$ *	-2.73	3.89	-4.06
Au|Pyr|2P|NH_2 *	-2.86	4.23	-3.86
Au|CN|2P|NH_2 *	-1.76	3.77	-3.23
Au|Pyr|2P|H *	-3.37	5.55	-3.05
Au|S|2P|NH_2 #	-0.86	3.57	-2.43
Au|CN|2P|H *	-1.93	5.05	-2.12
Au|S|2P|H *	-1.02	4.68	-1.54
Au|S|2P|F *	-1.00	6.43	0.23
Au|Pyr|2P|CN *	-2.87	9.39	1.29
Au|CN|2P|CN *	-1.81	9.12	2.07
Au|S|2P|CN #	-0.93	8.83	2.62
Au|S|B1|NH_2 #	-3.80	7.09	-1.86
Au|S|B1|CN #	-3.96	10.21	1.02
Au|S|B2|NH_2 #	-0.43	2.87	-2.68
Au|S|B2|CN #	-0.43	7.23	1.57
Au|S|2T|NH_2 #	-0.45	3.01	-2.58
Au|S|2T|CN #	-0.47	7.66	1.95
Au|S|B3|NH_2 #	-0.40	2.90	-2.63
Au|S|B3|CN #	-0.39	7.53	1.89
Au|S|B4|NH_2 #	-0.51	2.77	-2.86
Au|S|B4|CN #	-0.51	8.19	2.42

Table 2. Electronic properties of three SAMs on Au(111); data for the flat metal surface are compared to those for the SAM bonded through a Au ad-atom in the *fcc*-hollow position. The bond dipole, BD, the distance between the Fermi level and the HOPS, ΔE_{HOPS}, the ionization potential, IP_{SAM}, and the SAM-induced work-function modification, $\Delta\Phi$, are listed. In the presence of ad-atoms, $\Delta\Phi$ is calculated according to $\Delta\Phi = BD_{SH} + \Delta E_{vac} + \Delta\Phi_{ad\text{-}atom}$ to account for the effect of the ad-atoms on the work function; $\Delta\Phi_{ad\text{-}atom}$ = -0.52eV in all three cases; otherwise Eq. (7) is used to determine $\Delta\Phi$.

Systems	BD [eV]	ΔE_{HOPS} [eV]	IP_{SAM} [eV]	$\Delta\Phi$ [eV]
Au|S|2P|NH_2	-1.19	-0.86	3.57	-2.43
Au_{ad}|S|2P|NH_2	-0.25	-0.17	3.24	-2.13
Au|S|2P|H	-1.16	-1.02	4.68	-1.54
Au_{ad}|S|2P|H	-0.09	-0.18	4.46	-0.92
Au|S|2P|CN	-1.17	-0.90	8.68	2.58
Au_{ad}|S|2P|CN	-0.19	-0.17	8.44	3.07

((Author bio(s), max. 75 words))

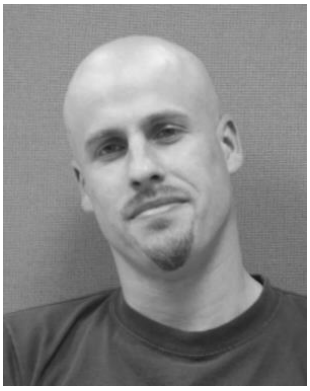

Georg Heimel received his Ph.D. in Physics (2003) from the Graz University of Technology in Austria. As recipient of an Erwin-Schrödinger (2004) and a Marie-Curie Fellowship (2006), he pursued his postdoctoral work at the Georgia-Institute of Technology (2004-2007) and the Massachusetts Institute of Technology (2007-2008). Currently based at the Institute of Physics of the Humboldt-Universität zu Berlin (Germany), he focuses on computational studies of organic/inorganic and organic/organic interfaces.

Ferdinand Rissner received his M.Sc. in Physics (2009) from the Graz University of Technology in Austria. He is currently a Ph.D. student in the group of Egbert Zojer working on the simulation of metal/organic and organic/organic interfaces.

Egbert Zojer received his Ph.D. in Physics (1999) from the Graz University of Technology, where he was appointed Associate Professor in 2002. On a leave from Graz, he worked for one year (2002-2003) as at the University of Arizona and for two years (2003-2005) at the Georgia Institute of Technology with Jean-Luc Brédas. His current research focuses on the computational investigation of organic/inorganic interfaces and the application of interface modifications in organic transistors.

.

Author Photograph(s) ((40 mm broad, 50 mm high))

The table of contents entry should be fifty to sixty words long, written in the present tense, and refer to the chosen figure.
Progress in modeling the electronic properties of π-conjugated self-assembled monolayers (SAMs) on metals is reported. Particular emphasis is put on the impact of the chemical composition of the SAM-forming molecules on key interfacial quantities such as the SAM-induced work-function modification and the energy-level alignment at metal/SAM and metal/SAM/organic-semiconductor junctions.

Keyword (see list)
(http://www3.interscience.wiley.com/journal/10008336/home/2089_toc_key.pdf)
Electronic Structure, Self Assembly, Monolayers, Organic Electronics, Structure-Property Relationships

Authors:
By *Georg Heimel,* Ferdinand Rissner,* and *Egbert Zojer**

Title:
Modeling the electronic properties of π-conjugated self-assembled monolayers.

ToC figure ((55 mm broad, 50 mm high, or 110 mm broad, 20 mm high))

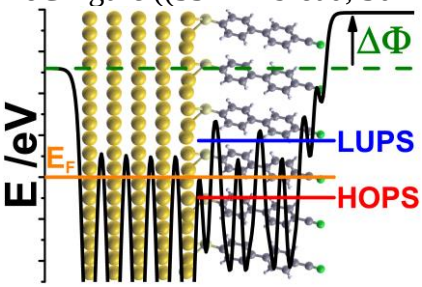

[1] J.-M. Lehn, *Angew. Chem., Int. Ed.* **1990**, *29*, 1304.

[2] M. Böhringer, K. Morgenstern, W.-D. Schneider, R. Berndt, F. Mauri, A. De Vita, R. Car, *Phys. Rev. Lett.* **1999**, *83*, 324.

[3] G. Tomba, L. C. Ciacchi, A. De Vita, *Adv. Mater.* **2009**, *21*, 1055.

[4] M. Ruben, J. Rojo, F. J. Romero-Salguero, L. H. Uppadine, J.-M. Lehn, *Angew. Chem., Int. Ed.* **2004**, *43*, 3644.

[5] U. Schlickum, R. Decker, F. Klappenberger, G. Zoppellaro, S. Klyatskaya, M. Ruben, I. Silanes, A. Arnau, K. Kern, H. Brune, J. V. Barth, *Nano Lett.* **2007**, *7*, 3813.

[6] G. Koller, S. Berkebile, J. R. Krenn, F. P. Netzer, M. Oehzelt, T. Haber, R. Resel, and M. G. Ramsey, *Nano Lett.* **2006**, 6, 1207.

[7] I. Fernandez-Torrente, S. Monturet, K. J. Franke, J. Fraxedas, N. Lorente, J. I. Pascual, *Phys. Rev. Lett.* **2007**, *99*, 176103.

[8] A. Ulman, *Chem. Rev.* **1996**, *96*, 1533.

[9] F. Schreiber, *Prog. Surf. Sci.* **2000**, 65, 151.

[10] F. Schreiber, *J. Phys.: Condens. Matter* **2004**, *16*, R881.

[11] J. J. Gooding, F. Mearns, W. R. Yang, J. Q. Liu, *Electroanal.* **2003**, *15*, 81.

[12] J. C. Love, L. A. Estroff, J. K. Kriebel, R. G. Nuzzo, G. M. Whitesides, *Chem. Rev.* **2005**, *105*, 1103.

[13] G. E. Poirier, *Chem. Rev.* **1997**, *97*, 1117.

[14] F. Schreiber, *Prog. Surf. Sci.* **2000**, *65*, 151.

[15] M. Kind, C. Wöll, *Prog. Surf. Sci.* **2009**, *84*, 230.

[16] G. Ashkenasy, D. Cahen, R. Cohen, A. Shanzer, A. Vilan, *Acc. Chem. Res.* **2002**, *35*, 121.

[17] A. Vilan, D. Cahen, *Trends Biotechnol.* **2002**, *20*, 22.

[18] C. Ganzorig, K.-J. Kwak, K. Yagi, M. Fujihira, *Appl. Phys. Lett.* **2001**, *79*, 272.

[19] E. L. Bruner, N. Koch, A. R. Span, S. L. Bernasek, A. Kahn, J. Schwartz, *J. Am. Chem. Soc.* **2002**, *124*, 3192.

[20] S. Onclin, B. J. Ravoo, and D. N. Reinhoudt, *Angew. Chem. Int. Ed.* **2005**, 44, 6282.

[21] G. K. Jennings, P. E. Laibinis, *Colloids Surf. A* **1996**, *116*, 105.

[22] J. Genzer, K. Efimenko, *Science* **2000**, *290*, 2130.

[23] P. Fontaine, D. Goguenheim, D. Deresmes, D. Vuillaume, M. Garet, F. Rondelez, *Appl. Phys. Lett.* **1993**, *62*, 2256.

[24] A. Facchetti, M. H. Yoon, T. J. Marks, *Adv. Mater.* **2005**, *17*, 1705.

[25] M.-H. Yoon, A. Facchetti, T. J. Marks, *Proc. Natl. Acad. Sci. U. S. A.* **2005**, *102*, 4678.

[26] M. Halik, H. Klauk, U. Zschieschang, G. Schmid, C. Dehm, M. Schutz, S. Maisch, F. Effenberger, M. Brunnbauer, F. Stellacci, *Nature* **2004**, *431*, 963.

[27] K. P. Pernstich, S. Haas, D. Oberhoff, C. Goldmann, D. J. Gundlach, B. Batlogg, A. N. Rashid, G. Schitter, *J. Appl. Phys.* **2004**, *96*, 6431.

[28] S. Kobayashi, T. Nishikawa, T. Takenobu, S. Mori, T. Shimoda, T. Mitani, H. Shimotani, N. Yoshimoto, S. Ogawa, Y. Iwasa, *Nature Mater.* **2004**, *3*, 317.

[29] L.-L. Chua, J. Zaumseil, J.-F. Chang, E. C. W. Ou, P. K. H. Ho, H. Sirringhaus, R. H. Friend, *Nature* **2005**, *434*, 194.

[30] X. F. Guo, M. Myers, S. X. Xiao, M. Lefenfeld, R. Steiner, G. S. Tulevski, J. Y. Tang, J. Baumert, F. Leibfarth, J. T. Yardley, M. L. Steigerwald, P. Kim, C. Nuckolls, *Proc. Natl. Acad. Sci. U. S. A.* **2006**, *103*, 11452.

[31] P. Pacher, A. Lex, V. Proschek, H. Etschmaier, E. Tchernychova, M. Sezen, U. Scherf, W. Grogger, G. Trimmel, C. Slugovc, E. Zojer, *Adv. Mater.* **2008**, *20*, 3143.

[32] G. S. Tulevski, Q. Miao, M. Fukuto, R. Abram, B. Ocko, R. Pindak, M. L. Steigerwald, C. R. Kagan, C. Nuckolls, *J. Am. Chem. Soc.* **2004**, *126*, 15048.

[33] E. C. P. Smits, S. G. J. Mathijssen, P. A. van Hal, S. Setayesh, T. C. T. Geuns, K. A. H. A. Mutsaers, E. Cantatore, H. J. Wondergem, O. Werzer, R. Resel, M. Kemerink, S. Kirchmeyer, A. M. Muzafarov, S. A. Ponomarenko, B. de Boer, P. W. M. Blom, D. M. de Leeuw, *Nature* **2008**, *455*, 956.

[34] C. Bock, D. V. Pham, U. Kunze, D. Käfer, G. Witte, C. Wöll, *J. Appl. Phys.* **2006**, *100*, 114517.

[35] K. Ihm, B. Kim, T. H. Kang, K. J. Kim, M. H. Joo, T. H. Kim, S. S. Yoon, S. Chung, *Appl. Phys. Lett.* **2006**, *89*, 033504.

[36] P. Marmont, N. Battaglini, P. Lang, G. Horowitz, J. Hwang, A. Kahn, C. Amato, and P. Calas P, *Org. Electronics* **2008**, 9, 419.

[37] B. H. Hamadani, D. A. Corley, J. W. Ciszek, J. M. Tour, and D. Natelson, *Nano Lett.* **2006**, 6 ,1303.

[38] I. H. Campbell, S. Rubin, T. A. Zawodzinski, J. D. Kress, R. L. Martin, D. L. Smith, N. N. Barashkov, J. P. Ferraris, *Phys. Rev. B* **1996**, *54*, R14321.

[39] I. H. Campbell, J. D. Kress, R. L. Martin, D. L. Smith, N. N. Barashkov, J. P. Ferraris, *Appl. Phys. Lett.* **1997**, *71*, 3528.

[40] B. de Boer, A. Hadipour, M. M. Mandoc, T. van Woudenbergh, P. W. M. Blom, *Adv. Mater.* **2005**, *17*, 621.

[41] *Molecular Electronics: Science and Technology* (Eds: A. Aviram, M. Ratner), Ann. N. Y. Acad. Sci., New York **1998**., Vol. 852.

[42] L. A. Bumm, J. J. Arnold, M. T. Cygan, T. D. Dunbar, T. P. Burgin, L. Jones, II, D. L. Allara, J. M. Tour, P. S. Weiss, *Science* **1996**, *271*, 1705.

[43] J. Chen, M. A. Reed, A. M. Rawlett, J. M. Tour, *Science* **1999**, *286*, 1550.

[44] J. G. Kushmerick, D. B. Holt, J. C. Yang, J. Naciri, M. H. Moore, R. Shashidhar, *Phys. Rev. Lett.* **2002**, *89*, 086802.

[45] D. J. Wold, C. D. Frisbie, *J. Am. Chem. Soc.* **2001**, *123*, 5549.

[46] A. Nitzan, M. A. Ratner, *Science* **2003**, *300*, 1384.

[47] H. B. Akkerman, P. W. M. Blom, D. M. de Leeuw, B. de Boer, *Nature* **2006**, *441*, 69.

[48] H. B. Akkerman, R. C. G. Naber, P. A. van Hal, P. W. M. Blom, D. M. de Leeuw, B. de Boer, *Proc. Natl. Acad. Sci. U.S.A* **2007**, *104*, 11161.

[49] A. J. Kronemeijer, H. B. Akkerman, T. Kudernac, B. J. van Wees, B. L. Feringa, P. W. M. Blom, B. de Boer, *Adv. Mater.* **2008**, *20*, 1467.

[50] Z. J. Donhauser, B. A. Mantooth, K. F. Kelly, L. A. Bumm, J. D. Monnell, J. J. Stapleton, D. W. Price, A. M. Rawlett, D. L. Allara, J. M. Tour, P. S. Weiss, *Science* **2001**, *292*, 2303.

[51] M. A. Reed, C. Zhou, C. J. Muller, T. P. Burgin, J. M. Tour, *Science* **1997**, *278*, 252.

[52] B. Q. Xu, N. J. J. Tao, *Science* **2003**, *301*, 1221.

[53] J. Park, A. N. Pasupathy, J. I. Goldsmith, C. Chang, Y. Yaish, J. R. Petta, M. Rinkoski, J. P. Sethna, H. D. Abruna, P. L. McEuen, D. C. Ralph, *Nature* **2002**, *417*, 722.

[54] L. Venkataraman, J. E. Klare, C. Nuckolls, M. S. Hybertsen, M. L. Steigerwald, *Nature* **2006**, *442*, 904.

[55] A. Natan, L. Kronik, H. Haick, R. T. Tung, *Adv. Mater.* **2007**, *19*, 4103.

[56] G. Heimel, L. Romaner, E. Zojer, J.-L. Bredas, *Acc. Chem. Res.* **2008**, *41*, 721.

[57] G. Heimel, L. Romaner, J. L. Bredas, E. Zojer, *Surf. Sci.* **2006**, *600*, 4548.

[58] A. Natan, Y. Zidon, Y. Shapira, L. Kronik, *Phys. Rev. B* **2006**, *73*, 193310.

[59] M. Sushko, L., A. Shluger, L., *Adv. Funct. Mater.* **2008**, *18*, 2228.

[60] P. C. Rusu, G. Giovannetti, G. Brocks, *J. Phys. Chem. C* **2007**, *111*, 14448.

[61] V. De Renzi, R. Rousseau, D. Marchetto, R. Biagi, S. Scandolo, U. del Pennino, *Phys. Rev. Lett.* **2005**, *95*, 046804.

[62] Q. Sun, A. Selloni, G. Scoles, *J. Phys. Chem. B* **2005**, *110*, 3493.

[63] J.-g. Wang, E. Prodan, R. Car, A. Selloni, *Phys. Rev. B* **2008**, *77*, 245443.

[64] J. Neugebauer, M. Scheffler, *Phys. Rev. B* **1992**, *46*, 16067.

[65] A. Natan, L. Kronik, Y. Shapira, *Appl. Surf. Sci.* **2006**, *252*, 7608.

[66] K. Hummer, P. Puschnig, C. Ambrosch-Draxl, *Phys. Rev. B* **2003**, *67*, 184105.

[67] Of course, such a monolayer does not actually exist, but its properties are crucial for understanding the electronic structure of an actual SAM.

[68] Classical Electrodynamics, 3rd edition, John David Jackson, John Wiley & Sons, Inc.

[69] H. Ishii, K. Sugiyama, E. Ito, K. Seki, *Adv. Mater.* **1999**, *11*, 605.

[70] L. Romaner, G. Heimel, C. Ambrosch-Draxl, E. Zojer, *Adv. Funct. Mater.* **2008**, *18*, 3999.

[71] J. Topping, *Proc. R. Soc. London Ser. A* **1927**, *114*, 67.

[72] J. R. Macdonald, C. A. Barlow, *J. Chem. Phys.* **1963**, 39, 412.

[73] D. M. Taylor, G. F. Bayes, *Phys. Rev. E* **1994**, 49, 1439.

[74] O. Gershevitz, C. N. Sukenik, J. Ghabboun, D. Cahen, *J. Am. Chem. Soc.* **2003**, *125*, 4730.

[75] H. Fukagawa, H. Yamane, S. Kera, K. K. Okudaira, N. Ueno, *Phys. Rev. B* **2006**, *73*, 041302.

[76] D. Cornil, Y. Olivier, V. Geskin, J. Cornil, *Adv. Funct. Mater.* **2007**, *17*, 1143.

[77] Finite size effects actually even result in inappropriate dependencies of ε^{eff} on the packing density when directly applying Eq. 2 as shown in Ref. [70].

[78] G. Heimel, L. Romaner, J. L. Bredas, E. Zojer, *Phys. Rev. Lett.* **2006**, *96*, 196806.

[79] G. Heimel, L. Romaner, E. Zojer, J. L. Bredas, *Nano Lett.* **2007**, *7*, 932.

[80] M. Hasan, D. Bethell, M. Brust, *J. Am. Chem. Soc.* **2002**, *124*, 1132.

[81] The actual SAM forming process of dynamic adsorption, desorption, migration and rearrangement of molecules in solution or in vacuum is of course different, but the used conceptual description provides significantly more fundamental insight into the SAM-electronics.

[82] M. Malicki, Z. Guan, S. D. Ha, G. Heimel, S. Barlow, M. Rumi, A. Kahn, S. R. Marder, *Langmuir* **2009**, *25*, 7967.

[83] A. Shaporenko, M. Elbing, A. Baszczyk, C. von Hanisch, M. Mayor, M. Zharnikov, *J. Phys. Chem. B* **2006**, *110*, 4307.

[84] P. C. Rusu, G. Brocks, *Phys. Rev. B* **2006**, *74*, 073414.

[85] P. C. Rusu, G. Brocks, *J. Phys. Chem. B* **2006**, *110*, 22628.

[86] The H-layer does not describe the actual chemical processes upon bonding of individual SAM-forming molecules. For example, for calculating binding energies the formation of H_2 would have to be considered. Instead, ρ_H is necessary to describe what happens in a gedankenexperiment when for the whole SAM the S-H bonds are replaced by S-Au bonds.

[87] P. Maksymovych, D. C. Sorescu, J. T. Yates, *J. Phys. Chem. B* **2006**, *110*, 21161.

[88] P. Maksymovych, D. B. Dougherty, *Surf. Sci.* **2008**, *602*, 2017.

[89] J.-G. Zhou, F. Hagelberg, *Phys. Rev. Lett.* **2006**, *97*, 045505.

[90] L. Kankate, A. Turchanin, A. Gölzhäuser, *Langmuir* **2009**, *25*, 10435.

[91] D. J. Lavrich, S. M. Wetterer, S. L. Bernasek, G. Scoles, *J. Phys. Chem. B* **1998**, *102*, 3456.

[92] G. M. Whitesides, P. E. Laibinis, *Langmuir* **1990**, *6*, 87.

[93] N. Camillone, C. E. D. Chidsey, G. Y. Liu, G. Scoles, *J. Chem. Phys.* **1993**, *98*, 3503.

[94] C. A. Alves, E. L. Smith, M. D. Porter, *J. Am. Chem. Soc.* **1992**, *114*, 1222.

[95] C. A. Widrig, C. A. Alves, M. D. Porter, *J. Am. Chem. Soc.* **1991**, *113*, 2805.

[96] R. G. Nuzzo, B. R. Zegarski, L. H. Dubois, *J. Am. Chem. Soc.* **1987**, *109*, 733.

[97] J. Gottschalck, B. Hammer, *J. Chem. Phys.* **2002**, *116*, 784.

[98] Y. Yourdshahyan, H. K. Zhang, A. M. Rappe, *Phys. Rev. B* **2001**, *6308*, 081405.

[99] Y. Morikawa, T. Hayashi, C. C. Liew, H. Nozoye, *Surf. Sci.* **2002**, *507*, 46.

[100] Y. P. Cao, Q. F. Ge, D. J. Dyer, L. C. Wang, *J. Phys. Chem. B* **2003**, *107*, 3803.

[101] P. Fenter, A. Eberhardt, P. Eisenberger, *Science* **1994**, *266*, 1216.

[102] P. Fenter, F. Schreiber, L. Berman, G. Scoles, P. Eisenberger, M. J. Bedzyk, *Surf. Sci.* **1998**, *413*, 213.

[103] M. S. Yeganeh, S. M. Dougal, R. S. Polizzotti, P. Rabinowitz, *Phys. Rev. Lett.* **1995**, *74*, 1811.

[104] R. Staub, M. Toerker, T. Fritz, T. Schmitz-Hubsch, F. Sellam, K. Leo, *Langmuir* **1998**, *14*, 6693.

[105] J. Noh, M. Hara, *Langmuir* **2000**, *16*, 2045.

[106] H. Grönbeck, A. Curioni, W. Andreoni, *J. Am. Chem. Soc.* **2000**, *122*, 3839.

[107] Y. Yourdshahyan, A. M. Rappe, *J. Chem. Phys.* **2002**, *117*, 825.

[108] T. Hayashi, Y. Morikawa, H. Nozoye, *J. Chem. Phys.* **2001**, *114*, 7615.

[109] M. C. Vargas, P. Giannozzi, A. Selloni, G. Scoles, *J. Phys. Chem. B* **2001**, *105*, 9509.

[110] D. Fischer, A. Curioni, W. Andreoni, *Langmuir* **2003**, *19*, 3567.

[111] J. G. Zhou, Q. L. Williams, F. Hagelberg, *Phys. Rev. B* **2007**, *76*, 075408.

[112] H. Kondoh, M. Iwasaki, T. Shimada, K. Amemiya, T. Yokoyama, T. Ohta, M. Shimomura, S. Kono, *Phys. Rev. Lett.* **2003**, *90*, 066102.

[113] M. G. Roper, M. P. Skegg, C. J. Fisher, J. J. Lee, V. R. Dhanak, D. P. Woodruff, R. G. Jones, *Chem. Phys. Lett.* **2004**, *389*, 87.

[114] M. Yu, N. Bovet, C. J. Satterley, S. Bengio, K. R. J. Lovelock, P. K. Milligan, R. G. Jones, D. P. Woodruff, V. Dhanak, *Phys. Rev. Lett.* **2006**, *97*, 166102.

[115] F. P. Cometto, P. Paredes-Olivera, V. A. Macagno, E. M. Patrito, *J. Phys. Chem. B* **2005**, *109*, 21737.

[116] E. Torres, P. U. Biedermann, A. T. Blumenau, *Int. J. Quant. Chem.* **2009**, *109*, 3466.

[117] J. V. Barth, H. Brune, G. Ertl, R. J. Behm, *Phys. Rev. B* **1990**, *42*, 9307.

[118] C. Wöll, S. Chiang, R. J. Wilson, P. H. Lippel, *Phys. Rev. B* **1989**, *39*, 7988.

[119] P. Maksymovych, D. C. Sorescu, J. T. Yates, *Phys. Rev. Lett.* **2006**, *97*, 146103.

[120] R. Mazzarello, A. Cossaro, A. Verdini, R. Rousseau, L. Casalis, M. F. Danisman, L. Floreano, S. Scandolo, A. Morgante, G. Scoles, *Phys. Rev. Lett.* **2007**, *98*, 016102.

[121] A. Cossaro, R. Mazzarello, R. Rousseau, L. Casalis, A. Verdini, A. Kohlmeyer, L. Floreano, S. Scandolo, A. Morgante, M. L. Klein, G. Scoles, *Science* **2008**, *321*, 943.

[122] A. Chaudhuri, T. J. Lerotholi, D. C. Jackson, D. P. Woodruff, V. Dhanak, *Phys. Rev. Lett.* **2009**, *102*, 126101.

[123] A. Cossaro, L. Floreano, A. Verdini, L. Casalis, A. Morgante, *Phys. Rev. Lett.* **2009**, *103*, 119601.

[124] A. Chaudhuri, T. J. Lerotholi, D. C. Jackson, D. P. Woodruff, V. Dhanak, *Phys. Rev. Lett.* **2009**, *103*, 119602.

[125] D. C. Jackson, A. Chaudhuri, T. J. Lerotholi, D. P. Woodruff, R. G. Jones, V. R. Dhanak, *Surf. Sci.* **2009**, *603*, 807.

[126] J. G. Wang, A. Selloni, *J. Phys. Chem. C* **2007**, *111*, 12149.

[127] E. Torres, A. T. Blumenau, P. U. Biedermann, *Phys. Rev. B* **2009**, *79*, 075440.

[128] G. Nenchev, B. Diaconescu, F. Hagelberg, K. Pohl, *Phys. Rev. B* **2009**, *80*, 081401.

[129] H. Kondoh, C. Kodama, H. Sumida, H. Nozoye, *J. Chem. Phys.* **1999**, *111*, 1175.

[130] G. E. Poirier, *Langmuir* **1999**, *15*, 1167.

[131] J. Noh, M. Hara, *Langmuir* **2001**, *17*, 7280.

[132] G. E. Poirier, E. D. Pylant, *Science* **1996**, *272*, 1145.

[133] M. H. Dishner, J. C. Hemminger, F. J. Feher, *Langmuir* **1997**, *13*, 2318.

[134] K. Edinger, A. Golzhauser, K. Demota, C. Wöll, M. Grunze, *Langmuir* **1993**, *9*, 4.

[135] G. E. Poirier, M. J. Tarlov, *Langmuir* **1994**, *10*, 2853.

[136] L. M. Molina, B. Hammer, *Chem. Phys. Lett.* **2002**, *360*, 264.

[137] Y. Morikawa, C. C. Liew, H. Nozoye, *Surf. Sci.* **2002**, *514*, 389.

[138] F. T. Arce, M. E. Vela, R. C. Salvarezza, A. J. Arvia, *Langmuir* **1998**, *14*, 7203.

[139] F. T. Arce, M. E. Vela, R. C. Salvarezza, A. J. Arvia, *J. Chem. Phys.* **1998**, *109*, 5703.

[140] G. E. Poirier, M. J. Tarlov, H. E. Rushmeier, *Langmuir* **1994**, *10*, 3383.

[141] G. E. Poirier, M. J. Tarlov, *J. Phys. Chem.* **1995**, *99*, 10966.

[142] J. Nara, S. Higai, Y. Morikawa, T. Ohno, *J. Chem. Phys.* **2004**, *120*, 6705.

[143] G. H. Yang, G. Y. Liu, *J. Phys. Chem. B* **2003**, *107*, 8746.

[144] P. Maksymovych, J. T. Yates, *J. Am. Chem. Soc.* **2008**, *130*, 7518.

[145] D. Käfer, G. Witte, P. Cyganik, A. Terfort, C. Wöll, *J. Am. Chem. Soc.* **2006**, *128*, 1723.

[146] G. Heimel, L. Romaner, E. Zojer, and J. L. Brédas, *Proc. SPIE* **2008**, Vol. 6999, 699919.

[147] G. Witte, S. Lukas, P. S. Bagus, C. Wöll, *Appl. Phys. Lett.* **2005**, *87*, 263502.

[148] L. Romaner, G. Heimel, E. Zojer, *Phys. Rev. B* **2008**, *77*, 045113.

[149] While the interfacial charge rearrangements upon SAM adsorption are actually a series of small consecutive dipoles, an equivalent single dipole can, in principle, be determined through Eq (1) that gives rise to a potential-energy step of the same magnitude as BD (see Ref. [148]).

[150] L. Romaner, G. Heimel, M. Gruber, J. L. Bredas, E. Zojer, *Small* **2006**, 2, 1468.

[151] This can be inferred, for example, by massive changes of the "right" ionization potentials of the non-bonded SAMs compared to the bonded ones.

[152] W. Azzam, C. Fuxen, A. Birkner, H. T. Rong, M. Buck, C. Wöll, *Langmuir* **2003**, *19*, 4958.

[153] T. Y. B. Leung, P. Schwartz, G. Scoles, F. Schreiber, A. Ulman, *Surf. Sci.* **2000**, 458, 34.

[154] G. Andreasen, M. E. Vela, R. C. Salvarezza, A. J. Arvia, *J. Electroanal. Chem.* **1999**, *467*, 230.

[155] D. Mayer, T. Dretschkow, K. Ataka, T. Wandlowski, *J. Electroanal. Chem.* **2002**, *524*, 20.

[156] G. Andreasen, M. E. Vela, R. C. Salvarezza, A. J. Arvia, *Langmuir* **1997**, *13*, 6814.

[157] B. Kim, J. M. Beebe, Y. Jun, X.-Y. Zhu, C. D. Frisbie, *J. Am. Chem. Soc.* **2006**, *128*, 4970.

[158] C. D. Zangmeister, S. W. Robey, R. D. van Zee, J. G. Kushmerick, J. Naciri, Y. Yao, J. M. Tour, B. Varughese, B. Xu, J. E. Reutt-Robey, *J. Phys. Chem. B* **2006**, *110*, 17138.

[159] J. J. Stapleton, T. A. Daniel, S. Uppili, O. M. Cabarcos, J. Naciri, R. Shashidhar, D. L. Allara, *Langmuir* **2005**, *21*, 11061.

[160] Y. Gilman, P. B. Allen, M. S. Hybertsen, *J. Phys. Chem. C* **2008**, *112*, 3314.

[161] D. Käfer, A. Bashir, G. Witte, *J. Phys. Chem. C* **2007**, *111*, 10546.

[162] A. Shaporenko, P. Cyganik, M. Buck, A. Terfort, M. Zharnikov, *J. Phys. Chem. B* **2005**, *109*, 13630.

[163] M. H. Dishner, J. C. Hemminger, F. J. Feher, *Langmuir* **1997**, *13*, 4788.

[164] A. Bashir, D. Käfer, J. Müller, C. Wöll, A. Terfort, G. Witte, *Angew. Chem. Int. Ed.* **2008**, *47*, 5250.

[165] S. Braun, W. R. Salaneck, M. Fahlman, *Adv. Mater.* **2009**, *21*, 1450.

[166] N. Koch, *Chem. Phys. Chem.* **2007**, *8*, 1438.

[167] A. Kahn, N. Koch, W. Y. Gao, *J. Polym. Sci., Part B* **2003**, *41*, 2529.

[168] D. M. Alloway, M. Hofmann, D. L. Smith, N. E. Gruhn, A. L. Graham, R. Colorado, V. H. Wysocki, T. R. Lee, P. A. Lee, N. R. Armstrong, *J. Phys. Chem. B* **2003**, *107*, 11690.

[169] R. W. Zehner, B. F. Parsons, R. P. Hsung, L. R. Sita, *Langmuir* **1999**, *15*, 1121.

[170] D. Fragouli, T. N. Kitsopoulos, L. Chiodo, F. Della Sala, R. Cingolani, S. G. Ray, R. Naaman, *Langmuir* **2007**, *23*, 6156.

[171] Q. Sun, A. Selloni, *J. Phys. Chem. A* **2006**, *110*, 11396.

[172] L.J. Wang, G. M. Rangger, L. Romaner, G. Heimel, T. Bučko, Z. Y. Ma, Q. K. Li, Z. Shuai, and E. Zojer, Advanced Functional Materials, available on-line.

[173] G. Heimel, E. Zojer, L. Romaner, J.-L. Bredas, F. Stellacci, *Nano Lett.* **2009**, *9*, 2559.

[174] What actually matters is the "local" polarizability of the head-group substituent and the adjacent part of the molecular backbone (see Figure 4), underlining again the need for introducing finite-size effects into the Topping model [70].

[175]The resulting negative work-function would, however, not actually be possible.

[176] S. Sze, K.K. Ng, "Physics of semiconductor devices"

[177] The qualitative conclusions do not change independent of whether one is performing the calculations in a spin polarized or non-polarized manner as discussed in the supporting information section of Ref. [173].

[178] N. Crivillers, C. Munuera, M. Mas-Torrent, C. Simao, S. T. Bromley, C. Ocal, C. Rovira, J. Veciana, *Adv. Mater.* **2009**, *21*, 1177.

[179] R. Liu, S. H. Ke, H. U. Baranger, W. T. Yang, *J. Am. Chem. Soc.* **2006**, *128*, 6274.

[180] R. Liu, S. H. Ke, W. T. Yang, H. U. Baranger, *J. Chem. Phys.* **2006**, *124*, 024718.

[181] R. Liu, S. H. Ke, H. U. Baranger, W. T. Yang, *Nano Lett.* **2005**, *5*, 1959.

[182] R. Liu, S. H. Ke, W. Yang, H. U. Baranger, *J. Chem. Phys.* **2007**, *127*, 141104.

[183] L. H. Yu, Z. K. Keane, J. W. Ciszek, L. Cheng, J. M. Tour, T. Baruah, M. R. Pederson, D. Natelson, *Phys. Rev. Lett.* **2005**, *95*, 256803.

[184] H. X. He, X. L. Li, N. J. Tao, L. A. Nagahara, I. Amlani, R. Tsui, *Phys. Rev. B* **2003**, *68*, 045302.

[185] I. V. Pobelov, Z. H. Li, T. Wandlowski, *J. Am. Chem. Soc.* **2008**, *130*, 16045.

[186] G. M. Rangger, L. Romaner, G. Heimel, E. Zojer, *Surf. Interface Anal.* **2008**, *40*, 371.

[187] P. Cyganik, M. Buck, W. Azzam, C. Wöll, *J. Phys. Chem. B* **2004**, *108*, 4989.

[188] W. Azzam, P. Cyganik, G. Witte, M. Buck, C. Wöll, *Langmuir* **2003**, *19*, 8262.

[189] P. Cyganik, M. Buck, T. Strunskus, A. Shaporenko, J. D. E. T. Wilton-Ely, M. Zharnikov, C. Wöll, *J. Am. Chem. Soc.* **2006**, *128*, 13868.

[190] T. Ishida, W. Mizutani, U. Akiba, K. Umemura, A. Inoue, N. Choi, M. Fujihira, H. Tokumoto, *J. Phys. Chem. B* **1999**, *103*, 1686.

[191] T. Ishida, W. Mizutani, N. Choi, U. Akiba, M. Fujihira, H. Tokumoto, *J. Phys. Chem. B* **2000**, *104*, 11680.

[192] L. L. Duan, S. J. Garrett, *Langmuir* **2001**, *17*, 2986.

[193] P. Cyganik, M. Buck, T. Strunskus, A. Shaporenko, G. Witte, M. Zharnikov, C. Wöll, *J. Phys. Chem. C* **2007**, *111*, 16909.

[194] I. Thom, M. Buck, *Surf. Sci.* **2005**, *581*, 33.

[195] K. Heister, H. T. Rong, M. Buck, M. Zharnikov, M. Grunze, L. S. O. Johansson, *J. Phys. Chem. B* **2001**, *105*, 6888.

[196] T. Felgenhauer, H. T. Rong, M. Buck, *J. Electroanal. Chem.* **2003**, *550*, 309.

[197] M. Zharnikov, S. Frey, H. Rong, Y. J. Yang, K. Heister, M. Buck, M. Grunze, *Phys. Chem. Chem. Phys.* **2000**, *2*, 3359.

[198] A. Shaporenko, M. Brunnbauer, A. Terfort, L. S. O. Johansson, M. Grunze, M. Zharnikov, *Langmuir* **2005**, *21*, 4370.

[199] H. T. Rong, S. Frey, Y. J. Yang, M. Zharnikov, M. Buck, M. Wuhn, C. Wöll, G. Helmchen, *Langmuir* **2001**, *17*, 1582.

[200] A. Shaporenko, M. Brunnbauer, A. Terfort, M. Grunze, M. Zharnikov, *J. Phys. Chem. B* **2004**, *108*, 14462.

[201] G. Heimel, L. Romaner, J. L. Brédas, E. Zojer, *Langmuir* **2007**, *24*, 474.

[202] V. Heine, *Phys. Rev.* **1965**, *138*, 1689.

[203] S. G. Louie, M. L. Cohen, *Phys. Rev. B* **1976**, *13*, 2461.

[204] S. G. Louie, J. R. Chelikowsky, M. L. Cohen, *Phys. Rev. B* **1977**, *15*, 2154.

[205] J. Tersoff, *Phys. Rev. Lett.* **1984**, *52*, 465.

[206] J. Y. Gui, D. A. Stern, D. G. Frank, F. Lu, D. C. Zapien, A. T. Hubbard, *Langmuir* **1991**, *7*, 955.

[207] S. C. Chang, I. Chao, Y. T. Tao, *J. Am. Chem. Soc.* **1994**, *116*, 6792.

[208] K. Heister, M. Zharnikov, M. Grunze, L. S. O. Johansson, *J. Phys. Chem. B* **2001**, *105*, 4058.

[209] O. Azzaroni, M. E. Vela, G. Andreasen, P. Carro, R. C. Salvarezza, *J. Phys. Chem. B* **2002**, *106*, 12267.

[210] P. A. Agron, T. A. Carlson, W. B. Dress, G. L. Nyberg, *J. Electron Spectrosc. Relat. Phenom.* **1987**, *42*, 313.

[211] P. E. Laibinis, G. M. Whitesides, D. L. Allara, Y. T. Tao, A. N. Parikh, R. G. Nuzzo, *J. Am. Chem. Soc.* **1991**, *113*, 7152.

[212] H. Kondoh, N. Saito, F. Matsui, T. Yokoyama, T. Ohta, H. Kuroda, *J. Phys. Chem. B* **2001**, *105*, 12870.

[213] F. Bussolotti, M. G. Betti, C. Mariani, *Phys. Rev. B* **2006**, *74*, 125422.

[214] J. C. Love, D. B. Wolfe, R. Haasch, M. L. Chabinyc, K. E. Paul, G. M. Whitesides, R. G. Nuzzo, *J. Am. Chem. Soc.* **2003**, *125*, 2597.

[215] K. L. Murphy, W. T. Tysoe, D. W. Bennett, *Langmuir* **2004**, *20*, 1732.

[216] J. J. Stapleton, T. A. Daniel, S. Uppili, O. M. Cabarcos, J. Naciri, R. Shashidhar, D. L. Allara, *Langmuir* **2005**, *21*, 11061.

[217] D. A. Stern, E. Wellner, G. N. Salaita, L. Lagurendavidson, F. Lu, N. Batina, D. G. Frank, D. C. Zapien, N. Walton, A. T. Hubbard, *J. Am. Chem. Soc.* **1988**, *110*, 4885.

[218] C. Alonso, M. F. Lopez, A. Gutierrez, M. L. Escudero, *Surf. Interface Anal.* **2000**, *30*, 359.

[219] T. H. Lin, T. P. Huang, Y. L. Liu, C. C. Yeh, Y. H. Lai, W. H. Hung, *J. Phys. Chem. B* **2005**, *109*, 14079.

[220] M. L. Chabinyc, X. X. Chen, R. E. Holmlin, H. Jacobs, H. Skulason, C. D. Frisbie, V. Mujica, M. A. Ratner, M. A. Rampi, G. M. Whitesides, *J. Am. Chem. Soc.* **2002**, *124*, 11730.

[221] L. Tamam, H. Kraack, E. Sloutskin, B. M. Ocko, P. S. Pershan, A. Ulman, M. Deutsch, *J. Phys. Chem. B* **2005**, *109*, 12534.

[222] H. Rieley, G. K. Kendall, R. G. Jones, D. P. Woodruff, *Langmuir* **1999**, *15*, 8856.

[223] M. Yu, D. P. Woodruff, N. Bovet, C. J. Satterley, K. Lovelock, R. G. Jones, V. Dhanak, *J. Phys. Chem. B* **2006**, *110*, 2164.

[224] D. P. Woodruff, *Appl. Surf. Sci.* **2007**, *254*, 76.

[225] G. M. He, *Phys. Rev. B* **2006**, *74*, 245421.

[226] M. Konopka, R. Rousseau, I. Stich, D. Marx, *Phys. Rev. Lett.* **2005**, *95*, 096102.

[227] V. Perebeinos, M. Newton, *Chem. Phys.* **2005**, *319*, 159.

[228] J. F. Kang, A. Ulman, S. Liao, R. Jordan, G. H. Yang, G. Y. Liu, *Langmuir* **2001**, *17*, 95.

[229] S. Frey, V. Stadler, K. Heister, W. Eck, M. Zharnikov, M. Grunze, B. Zeysing, A. Terfort, *Langmuir* **2001**, *17*, 2408.

[230] H. B. Michaelson, *J. Appl. Phys.* **1977**, *48*, 4729.

[231] C. D. Zangmeister, L. B. Picraux, R. D. van Zee, Y. X. Yao, J. M. Tour, *Chem. Phys. Lett.* **2007**, *442*, 390.

[232] M. G. Betti, A. Kanjilal, C. Mariani, H. Vázquez, Y. J. Dappe, J. Ortega, F. Flores, *Phys. Rev. Lett.* **2008**, *100*, 027601.

[233] F. Rissner, G. M. Rangger, O. T. Hofmann, A. M. Track, G. Heimel, and E. Zojer, ACS Nano, available on-line.

[234] J. P. Perdew, M. Levy, *Phys. Rev. Lett.* **1983**, *51*, 1884.

[235] R. K. Khanna, Y. M. Jiang, B. Srinivas, Ch. B. Smithhart, and D. L. Wertz, *Chem. Mater.* **1993**, 5, 1792 and references therein.

[236] J. Grimme, M. Kreyenschmidt, F. Uckert, K. Müllen, and U. Scherf, *Adv. Mater.* **1995**, 7, 292.

[237] E. Zojer, J. Cornil, G. Leising, and J. L. Brédas, *Phys. Rev. B* **1999**, 59, 7957.

[238] J. Hwang, A. Wan, A. Kahn, *Mater. Sci. Eng. R* **2009**, *64*, 1.

[239] B. Bröker, R.-P. Blum, L. Beverina, O. T. Hofmann, M. Sassi, R. Ruffo, G. A. Pagani, G. Heimel, A. Vollmer, J. Frisch, J. P. Rabe, E. Zojer, N. Koch, *Chem. Phys. Chem.* **2009**, available on-line.

[240] M. Methfessel, A. T. Paxton, *Phys. Rev. B* **1989**, *40*, 3616.

[241] S. Kurtin, T. C. Mcgill, C. A. Mead, *Phys. Rev. Lett.* **1969**, *22*, 1433.

[242] M. Schlüter, *Phys. Rev. B* **1978**, *17*, 5044.

[243] J. Tersoff, *Phys. Rev. B* **1985**, *32*, 6968.

[244] K. Seki, E. Ito, H. Ishii, *Synth. Met.* **1997**, *91*, 137.

[245] A. Crispin, X. Crispin, M. Fahlman, M. Berggren, W. R. Salaneck, *Appl. Phys. Lett.* **2006**, *89*, 213503.

[246] In fact, for the –CN terminated SAMs (systems (9), (10), (11)), pinning of the LUMO-derived band of 2P occurs at the HOPS of the SAM, but at an entirely different energy.

[247] C. Tengstedt, W. Osikowicz, W. R. Salaneck, I. D. Parker, C.-H. Hsu, M. Fahlman, *Appl. Phys. Lett.* **2006**, *88*, 053502.

[248] S. Braun, M. P. de Jong, W. Osikowicz, W. R. Salaneck, *Appl. Phys. Lett.* **2007**, 91, 202108.

[249] M. Montalti, L. Prodi, N. Zaccheroni, R. Baxter, G. Teobaldi, F. Zerbetto, *Langmuir* **2003**, *19*, 5172.

[250] G. Teobaldi, F. Zerbetto, *J. Phys. Chem. C* **2007**, *111*, 13879.

[251] S. Rapino, F. Zerbetto, *Small* **2007**, *3*, 386.

[252] T. E. Dirama, J. A. Johnson, *Langmuir* **2007**, *23*, 12208.

[253] S. N. Patole, C. J. Baddeley, D. O'Hagan, N. V. Richardson, F. Zerbetto, L. A. Zotti, G. Teobaldi, W. A. Hofer, *J. Chem. Phys.* **2007**, *127*, 024702.

[254] R. Liu, S. H. Ke, H. U. Baranger, W. T. Yang, *J. Chem. Phys.* **2005**, *122*, 044703.

[255] L. A. Agapito, C. Cao, H. P. Cheng, *Phys. Rev. B* **2008**, *78*, 155421.